Theses   Electronic Theses and Dissertations

11-2023

RADIO EMISSION FROM LOW MASS ACTIVE GALACTIC NUCLEI

Ammara Aftab

RADIO EMISSION FROM LOW-MASS ACTIVE GALACTIC NUCLEI

Ammara Aftab

United Arab Emirates University

College of Science

Department of Physics

RADIO EMISSION FROM LOW-MASS ACTIVE GALACTIC NUCLEI

Ammara Aftab

This thesis is submitted in partial fulfillment of the requirements for the degree of Master of Science in Space Science

November 2023

Cover: Prediction for radio flux from six different fundamental planes for GN-z1, the farthest galaxy observed by James Web Space Telescope with telescope limits for SKA (solid line) and ngVLA (dashed line).

(Photo: By Ammara Aftab)

Declaration of Original Work

I, Ammara Aftab, the undersigned, a graduate student at the United Arab Emirates University (UAEU), and the author of this thesis entitled "*Radio Emission from low-mass Active galactic Nuclei*", hereby, solemnly declare that this is the original research work done by me under the supervision of Dr. Mohammad Abdul Latif, in the College of Science at UAEU. This work has not previously formed the basis for the award of any academic degree, diploma, or similar title at this or any other university. Any materials borrowed from other sources (whether published or unpublished) and relied upon or included in my thesis have been properly cited and acknowledged in accordance with appropriate academic conventions. I further declare that there is no potential conflict of interest with respect to the research, data collection, authorship, presentation, and/or publication of this thesis.

Student's Signature: _____

Date: 16th October 2023

Approval of the Master Thesis

This Master Thesis is approved by the following Examining Committee Members:

1) Advisor (Committee Chair): Dr. Mohammad Abdul Latif
   Title: Associate Professor
   Department of Physics
   College of Science

   Signature _____   Date ___05/12/2023_____

2) Member: Dr. Aquib Moin
   Title: Associate Professor
   Department of Physics
   College of Science

   Signature _____   Date ___06/12/2023_____

3) Member (External Examiner): Prof. Fazeel Khan
   Title: Full Professor
   Department of Space Science
   Institution: Institute of Space Technology, Islamabad, Pakistan

   Signature _____   Date ___07/12/2023_____

This Master Thesis is accepted by:

Dean of the College of Science: Professor Maamar Benkraouda

Signature _____

Date 5/6/2024 _____

Dean of the College of Graduate Studies: Professor Ali Al-Marzouqi

Signature _Ali Hassan_____

Date _____June 5, 2024_____

Abstract

Massive black holes of a few million to billion solar masses lurk at the centers of the most present-day massive galaxies but their origin is still unknown. The low mass galaxies ($M* \sim 3x10^9$ $M_\odot$) hosting black holes with masses ranging from 10^3 to 10^5 $M_\odot$ are ideal laboratories to test the models of black hole formation and they may help in understanding the co-evolution of central black holes with their host galaxies. In this thesis, we have developed a detailed theoretical model/framework to estimate the radio emission from low-mass active galactic nuclei (AGN). We also compute the contribution of radio emission from HII regions and supernova remnants in the host galaxy. Our estimated radio fluxes for AGN of 10^5 -10^7 $M_\odot$ range from 0.6-2000 nJy at redshift 10 assuming the Eddington limited accretion. The most recent observations by the James Webb Space Telescope (JWST) have unveiled the presence of low-mass AGN at high redshift. We predict that these newly observed sources can be detected in radio with upcoming radio telescopes such as the next-generation Very Large Array (ngVLA) and the Square Kilometer Array (SKA) for integration times of 1-100 hours. These observations will unambiguously confirm the existence of AGN.

Keywords: Active galactic nuclei, Black holes, Radio emission, Radio flux, Luminosity, Fundamental planes, Black hole masses, Accretion rates.

Title and Abstract (in Arabic)

انبعاث الراديو من نوى المجرة النشطة منخفضة الكتلة

الملخص

تكمن الثقوب السوداء الضخمة التي تتراوح كتلتها بين بضعة ملايين إلى مليار كتلة شمسية في مراكز المجرات الأكثر ضخامة في الوقت الحاضر، لكن أصلها لا يزال غير معروف. المجرات منخفضة الكتلة ($M* \sim 3x10^9\ M_\odot$) التي تستضيف ثقوبًا سوداء تتراوح كتلتها من 10^3 إلى $10^5\ M_\odot$ هي مختبرات مثالية لاختبار نماذج تكوين الثقب الأسود وقد تساعد في فهم التطور المشترك للثقوب السوداء المركزية مع مضيفها. المجرات. في هذه الأطروحة، قمنا بتطوير نموذج/إطار نظري مفصل لتقدير الانبعاثات الراديوية من نوى المجرة النشطة منخفضة الكتلة (AGN). نقوم أيضًا بحساب مساهمة الانبعاثات الراديوية من مناطق HII وبقايا المستعرات الأعظم في المجرة المضيفة. تتراوح تدفقاتنا الراديوية المقدرة لـ AGN البالغة 10^5- $10^7\ M_\odot$ من 0.6 إلى nJy 2000 عند الانزياح الأحمر 10 بافتراض تراكم Eddington المحدود. كشفت أحدث عمليات الرصد التي أجراها تلسكوب جيمس ويب الفضائي عن وجود نوى نشطة منخفضة الكتلة عند انزياح أحمر مرتفع. نتوقع أنه يمكن اكتشاف هذه المصادر المرصودة حديثًا في الراديو باستخدام التلسكوبات الراديوية القادمة مثل الجيل التالي من المصفوفة الكبيرة جدًا (ngVLA) ومصفوفة الكيلومتر المربع (SKA) لأوقات تكامل تتراوح من 1 إلى 100 ساعة. ستؤكد هذه الملاحظات بشكل لا لبس فيه وجود AGN.

مفاهيم البحث الرئيسية: نوى المجرة النشطة، الثقوب السوداء، الانبعاث الراديوي، التدفق الراديوي، اللمعان، المستويات الأساسية، كتل الثقب الأسود، معدلات التراكم.

Author Profile

Ammara Aftab is at present working as a Physics teacher for higher grades at Al Sanawbar School Al Ain. She has more than six years of experience teaching physics in high school. She has done her bachelor's degree in physics from International Islamic University Islamabad, Pakistan. She earned a gold medal during her bachelor's for her high academic performance throughout her degree program. She has also received a Professional Postgraduate Diploma in Teaching from Abu Dhabi University, Al Ain. During her internship, she worked at the Center for Astro, Particle, and Planetary Physics at New York University Abu Dhabi. Apart from all these academic achievements she has been doing a lot of social work as well. She worked as an RJ at a Relief Radio station in her hometown after the 2005 Earthquake in Pakistan to support relief and rehabilitation activities. Ammara is currently living with her family in Al Ain.

Acknowledgments

I would like to thank my committee for their guidance, support, and assistance throughout my preparation of this thesis, especially my advisor Dr. Mohammad Abdul Latif for his constant support and motivation.

Dedication

To my beloved parents and family, especially my husband and my son who have always been a great support for me.

Table of Contents

List of Tables

List of Figures

List of Abbreviations

AGN   Active Galactic Nuclei

BH   Black hole

DCBH   Direct Collapse Black Hole

FP   Fundamental Planes

IMBH   Intermediate Mass Black Hole

JWST   James Web Space Telescope

LMAGN   Low Mass Active Galactic Nuclei

ngVLA   Next Generation Very Large Array

NIR   Near Infrared

RST   Roman Space Telescope

SFR   Star Formation Rate

SKA   Square Kilometer Array

SMBH   Supermassive Black Hole

Chapter 1: Introduction

1.1 Overview

In this thesis, the primary objective of our research has been the development of a theoretical model for the computation of radio emissions originating from low-mass Active Galactic Nuclei (AGN). These emissions are subsequently compared with observational data obtained through radio observations. Our work is fundamentally geared towards enhancing our understanding of the characteristics of low-mass AGN, thus contributing to a more profound comprehension of the origins of supermassive black holes and their co-evolution with their host galaxies.

Chapter 1 serves as the introductory section of this thesis. Herein, we present a comprehensive overview of our research topic, providing context, elucidating the primary objectives, and contextualizing our work within the existing academic literature. In Chapter 2, we take a closer look at AGN. We'll discuss black holes, how they're formed, what they look like on the inside, and how they produce radio waves. This chapter helps us understand AGN better and explains the science behind its structure and the radio waves emission. Chapter 3 presents the mathematical model that supports our study. Within this chapter, we explain the utilization of fundamental plane equations for the estimation of radio flux emanating from the cores of black holes (BHs). Additionally, we provide an in-depth description of the mathematical expressions employed for calculating radio flux from AGN jets, drawing upon the methodology established by Yue et al. (2021), as detailed in Section 5 of this chapter. Furthermore, Sections 3 and 4 of this chapter offer a mathematical foundation for the estimation of radio flux originating from HII regions and supernova remnants. Chapter 4 is dedicated to the presentation of the results derived from our theoretical model. This chapter incorporates an exhaustive discussion of the obtained data, including detailed analyses of all graphical representations. The concluding part of this chapter encompasses our predictions regarding radio emissions from galaxies recently observed by the James Webb Space Telescope (JWST). Moreover, we provide predictions regarding their detectability using upcoming radio telescopes such as the Next Generation Very Large Array (ngVLA) and the Square Kilometer Array (SKA), considering various integration times. The final chapter of this thesis serves as a comprehensive summation of

our study, presenting a well-considered and knowledgeable conclusion. This chapter not only underlines the significance of our study, illuminating the original research questions and objectives but also presents a forward-looking perspective on the potential implications and applications of our work for future studies in this field.

1.2 Statement of the problem

Scientists have confirmed that nearly all galaxies have supermassive black holes at their centers, which are much larger and heavier than the sun (Kormendy & Ho, 2013). These black holes are relatively easy to study in our nearby universe. However, when it comes to studying these supermassive black holes in the early universe, it gets tricky, and we're still not sure how they form and evolve alongside their host galaxies (Latif & Khochfar, 2020). To solve this cosmic puzzle, we look at low-mass AGN. Low-mass AGN are testbeds for constraining the models of black hole formation and evolution. Their understanding is ultimately linked to the origin of supermassive black holes lurking at the centers of massive galaxies. Studying the radio properties of these low-mass AGN will help us understand the formation and evolution mechanism. Studying the radio flux from these low-mass AGN will unveil the nature of black hole seeds whether they were born heavy or light since low-mass AGN are expected to have changed little since their formation due to the quiescent nature of their host galaxies and supernova feedback suppresses black hole growth by ejecting cold gas needed to feed them. We will also make prediction for the observation of low-mass AGN by upcoming telescopes which will further enhance our understanding of the origin of supermassive black holes and their co-evolution with their host galaxy.

1.3 Research objectives

The prime objective of this research is to develop a detailed theoretical model that computes radio emissions from low-mass AGN. The model will estimate radio signals both from the core and jets of AGN and it will also estimate radio emission from HII regions and supernova remnants in the host galaxy. After verification of the model using previous work, we will use our model to estimate radio emissions from newly observed galaxies and will make predictions for their detection with upcoming radio telescopes such as ngVLA and SKA.

The main research objectives of this work are the following:

- Develop a theoretical model for radio emission from low-mass AGN.
- Study the correlation between radio emission from AGN and blackhole masses.
- Study the correlation between redshift and radio emission from AGN.
- Assess the potential contribution from HII regions and supernova remnants.
- Study the contribution from low mass AGN, HII regions, and Supernova and determine if the radio flux from AGN can be distinguished from radio flux from HII regions and Supernova remnants.
- Make predictions for newly observed galaxies by JWST, for their detection by ngVLA and SKA.

1.4 Relevant literature

Understanding the growth of massive black holes (MBHs) at high redshift is a major research focus in astrophysics. Supermassive black holes (SMBHs), with masses ranging from a few million to billions of solar masses, are commonly found at the centers of massive galaxies (Kormendy & Ho, 2013). Their origins have been a long-standing mystery in the field of astronomy. Recent observations have demonstrated that SMBHs are likely present at the centers of nearly all galaxies, and their properties show strong correlations with those of their host galaxies (Bonchi et al., 2013). Theoretical models of black hole formation suggest that SMBHs can originate from "seeds" with masses spanning from 10 to 100,000 times that of the Sun, known as light and heavy seeds. These seeds are believed to have formed in the early universe when conditions were favorable for their birth (Latif & Ferrara, 2016). However, many questions remain about the precise processes governing their formation and subsequent growth. One approach to investigating the origin of black holes is to study low-mass active black holes, often referred to as low-mass AGN, with masses in the range of 10^3 to 10^6 times that of the Sun. These AGN are expected to reside in low-mass galaxies with stellar masses of 10^9 $M_\odot$ (Greene, 2012).The key idea behind this approach is that low-mass galaxies hosting low-mass AGN have not undergone significant growth via major mergers. Additionally, the presence of supernova explosions and AGN feedback in these galaxies may hinder the growth of both the black holes and their host galaxies, preserving conditions closer to their

birth (Greene et al., 2020). In the context of this study, the focus is on deriving the radio signatures of low luminosity AGN. Radio observations are an essential tool in the study of AGN because they can provide insights into emission from relativistic jets, synchrotron radiation, and other phenomena associated with black hole activity. By analyzing radio emissions from low luminosity AGN in low mass galaxies, researchers aim to gain a better understanding of the early conditions of black hole formation and their co-evolution with their host galaxies.

AGN feedback plays a vital role in shaping the growth and evolution of supermassive black holes (SMBHs) and their host galaxies (Vito et al., 2022; Smolčić et al., 2009). AGN feedback can have either positive or negative impacts, depending on its influence on SMBH growth and galaxy evolution. One of the prominent effects of AGN feedback is the quenching of star formation, especially in the central regions of galaxies (Cresci & Maiolino, 2018). This process can essentially halt the formation of new stars. AGN are considered to be related to mechanisms capable of switching off star formation in the most massive galaxies, thus reproducing both the observed shape of the galaxy luminosity function and, the passive evolving nature of local massive galaxies (Bonchi et al., 2013). Observations indicate that the primary mechanism for hindering star formation is the depletion of gas for new star formation, without a sufficient supply of fresh gas (Cresci & Maiolino, 2018). Some models propose that AGN feedback is driven by the kinetic energy released by radio jets, with the strength of feedback being directly related to the AGN's radio luminosity (Croton et al., 2006; Cattaneo et al., 2006). Converting AGN radio luminosity into kinetic luminosity has been demonstrated to provide the necessary energy for this feedback mechanism (Bonchi et al., 2013). Hence, in this study, we will be looking into the radio flux from the jets of AGN.

In this study, we aim to estimate the radio emissions from AGN jets and their influence on the growth, evolution, and star formation within the host galaxy. The low-mass AGN (LMAGN) are low-luminosity systems with the typical Eddington ratios (L_{bol}/L_{Edd}) of $0.01 - 1$. The observational study of AGN with low-mass black holes can provide useful constraints on the initial conditions of galaxy evolution or the "seed" black holes from which the supermassive black holes eventually form. The first dedicated campaign to systematically search for AGN with black hole masses less than $10^6\,M_\odot$ was

carried out by (Greene & Ho, 2004). Their campaign found 19 low-mass galaxies and this sample was later expanded to a larger sample of 229 LMAGN (Greene & Ho, 2007). Dong et al. (2012) presented a new sample of 309 LMAGN using SDSS DR4 spectroscopic data. This sample has about 50% overlap with the Greene & Ho (2007) samples, and it consists of 61 newly discovered sources. With a comparatively lenient selection criterion, they were also able to find some low-mass AGN with lower accretion rates. More recently (Mezcua & Domínguez Sánchez, 2020) reported the discovery of 35 dwarf galaxies hosting radio AGN out to z ~ 3.4. Their galaxies are taken from the VLA-COSMOS 3 GHz Large Project, and all are star-forming. They found a range of AGN radio luminosities of L $_{AGN\ 1.4GHz}$ $10^{37} - 10^{40}$ erg/s and the bolometric 1.4 GHz luminosities of 10^{42} erg/s. The 3 GHz radio emission of most of the sources is compact and the jet powers range from Q $_{jet}$ ~ $10^{42} - 10^{44}$ erg/s. These values indicate that dwarf galaxies can host radio jets as powerful as those of massive radio galaxies (Mezcua & Prieto, 2014) whose jet mechanical feedback can strongly affect the formation of stars in the host galaxy. We conclude that AGN feedback can also have a very strong impact on dwarf galaxies, either triggering or hampering star formation and possibly the material available for BH growth. These observational studies suggest that low mass AGN exhibit a wide range of Eddington ratios and indicate a correlation between the radio loudness and bolometric luminosity, i.e., systems with low Eddington ratios are more radio loud. Also, the Eddington ratios are higher for AGN with lower black hole masses.

Motivated by the observational studies, we aimed to develop a physical model for radio emission from low-mass AGN which takes into account the radio contribution both from accretion disks and AGN jets. Our model explored a wide range of parameters such as black hole masses ($10^4 - 10^7$ M$_\odot$), Eddington ratios, redshift, and spectral indices. Our model is based on an empirically confirmed correlation between black hole mass, its X-ray luminosity, and 5 GHz nuclear luminosity known as the fundamental plane of the black hole. To make our model a comprehensive one we took different fundamental planes of (Merloni et al., 2003; Gültekin et al., 2014; Gültekin et al., 2009; Bonchi et al., 2013; Körding et al., 2006; Plotkin et al., 2012) and compared radio flux from them. We employed this model to predict radio emission from the direct collapse black holes (DCBH) at high redshift and checked its validity and compared our results with results

from (Whalen et al., 2020; Whalen et al., 2023 ; Whalen et al., 2021. This model was extended to take into account the emission from a radio jet by employing the framework developed by Yue & Ferrara (2021), originally taken from Bîrzan et al. (2008). In addition to this, we also assessed the potential contribution of radio flux from star formation in the host galaxy such as supernova remnants, and HII regions. Observations of star formation rates (SFRs) in galaxies provide vital clues to the physical nature of the galaxy and are key probes of the evolutionary histories of galaxies. Estimates from this model enabled us to understand the correlation between AGN accretion and their radio loudness.

Recent studies suggest that DCBHs could be detected in the near-infrared by the James Webb Space Telescope, Euclid, and the Roman Space Telescope. Several studies have examined the prospects for the detection of supermassive DCBHs in the near-infrared (NIR) by the James Webb Space Telescope (JWST), Euclid, and the Roman Space Telescope (RST). They found that DCBHs could be detected by JWST at $z < 20$ and by Euclid and RST at $z < 6$ - 8, although lensing by galaxy clusters and massive galaxies in their wide fields could extend these detections up to $z < 10 - 15$ (Whalen et al., 2020; Barrow et al., 2018). However, new radio telescopes with unprecedented sensitivities such as the SKA and ngVLA which are expected to be launched in a decade may open another window on the properties of AGN in the coming years. Using our model, we have made predictions for upcoming radio telescopes such as ngVLA and SKA. We have also applied our model to newly observed galaxies by JWST and predicted their detection by ngVLA and SKA. We took data from Maiolino et al. (2023) and Scoggins & Haiman. (2023) for these newly observed galaxies shown in Figure 1 and predicted Radio flux from the accretion disk of the black holes. The contribution from HII regions and Supernova remnants could not be estimated as these sources are newly observed, and much information is not available yet. Given that data regarding the star formation rate for these galaxies is currently unavailable, estimating the radio flux from HII regions and Supernova remnants remains a challenge. It is unclear whether the radio flux from these sources can be effectively distinguished from the radio flux originating from the Black Hole (BH). Looking ahead, as more information becomes accessible in the future, our model can be employed to estimate the radio flux emanating from HII regions and Supernova remnants within these galaxies. Such estimates would greatly enhance our understanding of the

evolution of these galaxies. In the coming years, the advent of advanced telescopes and observational tools is expected to usher in new opportunities for the study of low-mass AGN. These resources will enable researchers to delve deeper into the origins, formation, and evolution of these AGN, particularly at high redshifts. This progression promises to shed more light on the intricate dynamics at play within these galaxies.
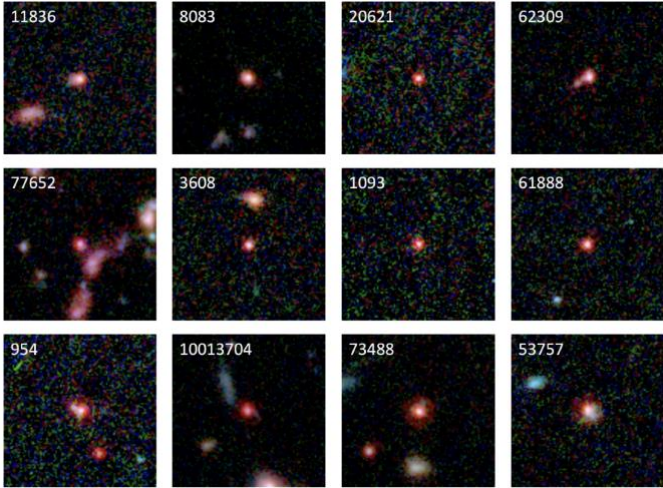

Figure 1: NIR Cam images of the selected AGN observed by JWST. Credit: (Maiolino et al., 2023)

Chapter 2: Active Galactic Nuclei: An Overview

2.1 What are AGN

Active Galactic Nuclei (AGN) represent exceptionally luminous and energetic central regions within galaxies as shown in Figure 2. These regions are primarily characterized by the intense emission of light, primarily originating from dust and gas as it falls into a SMBH located at the core of a galaxy. The cosmological significance of AGN is profound. Their immense energy output can have a substantial impact on the immediate galactic environment, potentially influencing the formation and evolution of galaxies (Plotkin et al., 2012; (Smolčić et al., 2009). AGN emit such an extraordinary amount of energy that they can often outshine the entire galaxy in which they reside (Tremaine, 2014). AGN are remarkable in their ability to emit radiation across the entire electromagnetic spectrum, spanning from radio waves to gamma rays. This radiation is generated by the interactions occurring in the vicinity of the central SMBH, as it accretes material from its surroundings. The matter spirals into the black hole due to frictional forces, causing the surrounding gas to heat up and emit radiation (Tremaine, 2014). The central engine of an AGN consists of key components, including the central supermassive black hole, an accretion disk formed from the material spiraling into the black hole, often accompanied by a corona, and, in many cases, relativistic jets (Körding et al., 2006). The presence of an AGN within a galaxy classifies it as an "active galaxy," and this has significant implications for the galaxy's overall characteristics and behavior. AGN serve as crucial subjects in the field of astrophysics and cosmology, offering insights into the universe's evolution and the processes involved in the release of immense energy and radiation from the vicinity of supermassive black holes.

AGN stands out as the most radiant and persistent source of electromagnetic radiation in the cosmos. Their remarkable luminosity makes them valuable tools for discovering distant celestial objects. Astronomers have categorized various types of AGN based on their observed characteristics. The term "active galactic nuclei" encompasses several intriguing subclasses, including quasars, blazars, and Seyfert galaxies. These classifications begin with their distances from Earth, Seyfert galaxies are relatively close, allowing us to readily observe and study the galaxies in their vicinity. In contrast, quasars,

named after "quasi-stellar radio sources," are exceptionally distant and appear as point-like sources, a label that can be somewhat misleading. The most potent AGNs are known as quasars, and they are responsible for the creation of extremely luminous galactic centers. We now know that bright active galactic nuclei are also surrounded by galaxies, but the galaxies' light is difficult to differentiate from the quasars' light as they emit more energy than any other object in the universe (Tremaine, 2014). A range of "active galaxies" classifications have been identified, including quasars, radio galaxies, and Seyfert galaxies. The observed energy emissions result from the accretion of matter onto a supermassive black hole, often with a mass many millions or even billions of times that of the Sun. As this matter spirals into the black hole due to high-speed collisions and friction, it becomes intensely heated and can outshine the remainder of the host galaxy as shown in Figure 2.
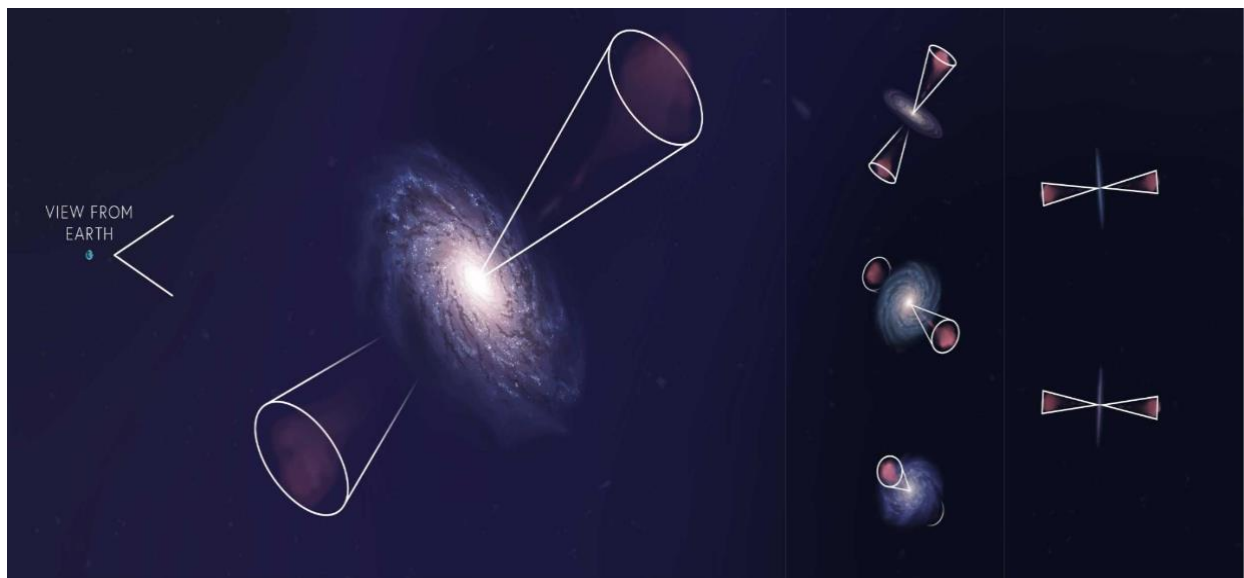
Figure 2: Figure showing AGN from different viewing angles. Photo credit: NASA

2.2 What is a black hole

Black holes are celestial entities renowned for their remarkable gravitational potency. They are characterized as regions in spacetime where gravitational forces are so overwhelmingly intense that they prohibit the escape of particles and electromagnetic radiation (Fabian & Lasenby, 2019). These enigmatic objects have captivated the attention

of astronomers and astrophysicists, as their study contributes significantly to elucidating the genesis and structure of the cosmos. Black holes possess an extraordinary gravitational field, from which even light cannot escape, bestowing upon them their characteristic nature. At the core of a black hole is the event horizon, a defining feature. The event horizon as shown in Figure 4 is a theoretical boundary beyond which any entity that traverses it becomes inexorably drawn into the black hole's grasp, with no possibility of return (Fabian & Lasenby, 2019). The size of a black hole, and hence the dimensions of its event horizon, is contingent upon its mass. Larger masses engender correspondingly larger black holes and event horizons. Supermassive black holes, endowed with immense mass and gravitational force, are situated at the centers of galaxies, while stellar-mass black holes, originating from the gravitational collapse of massive stars, occupy various locations within galaxies. The term "black hole" is metaphorical, representing a phenomenon that resembles a hole from which nothing can escape due to its potent gravitational field.
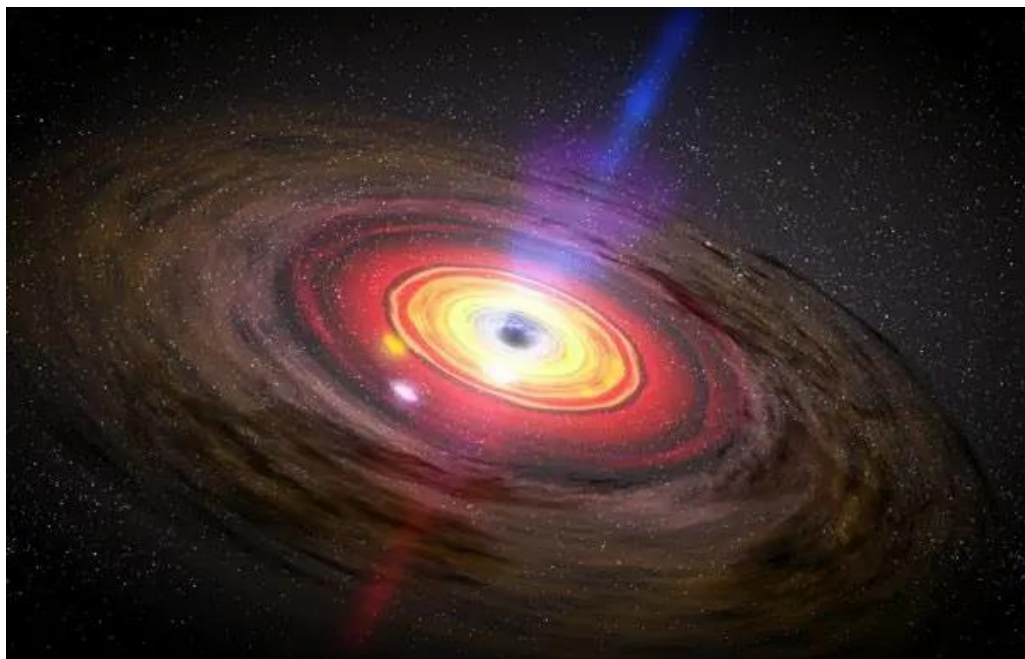
Figure 3: Artist concept of matter swirling around a black hole. Credits: NASA/Dana Berry/Skyworks Digital

An established astronomical fact is that nearly all known galaxies in the universe harbor a black hole in their nucleus (Tremaine, 2014). These central black holes, often

referred to as supermassive black holes, exert a profound influence on galactic dynamics and evolution. An exemplar of such an entity is Sagittarius A*, situated at the heart of our Milky Way galaxy (Zahid et al., 2023; Tremaine, 2014). Sagittarius A* has a mass of approximately 4.3 million times that of the Sun and resides within the Sagittarius constellation.

2.3 Anatomy of black holes

Till now scientists have discovered different types of black holes having different masses and other properties, but they all possess almost similar structures having the following common features:
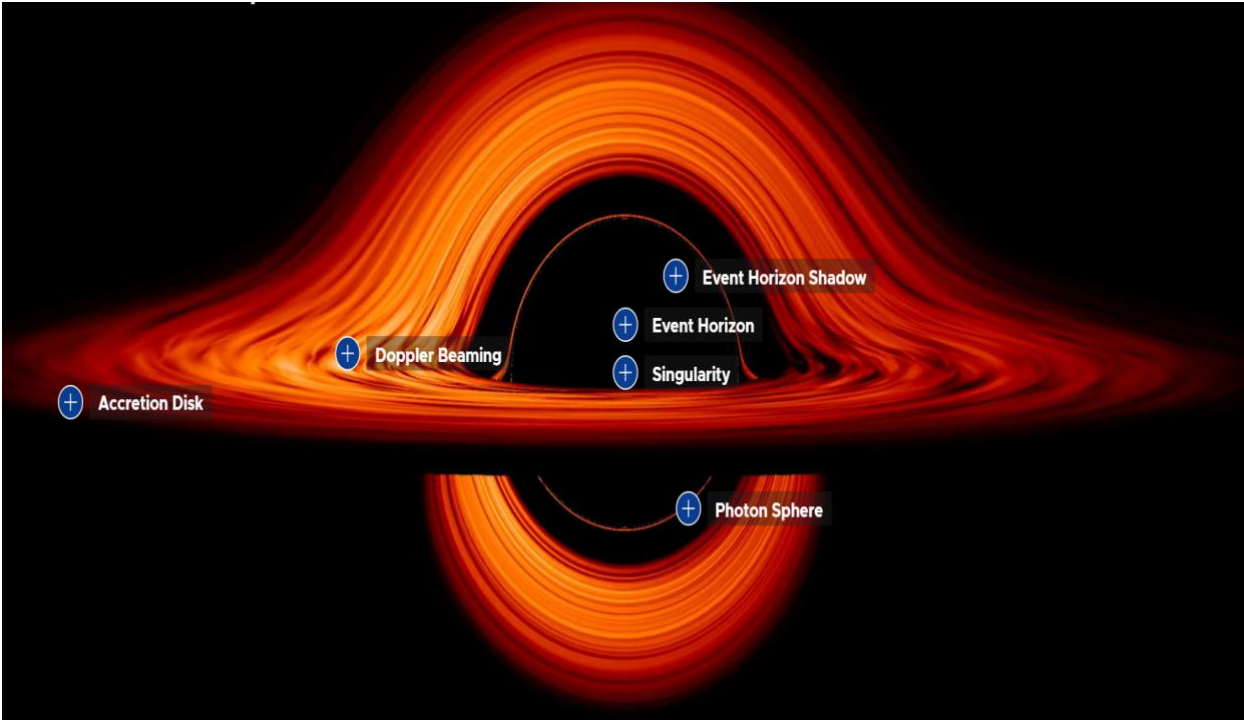
Figure 4: Figure showing different components of a Black hole. Credits: NASA's Goddard Space Flight Center/Jeremy Schnittman

2.3.1 Event of horizon

Light is the fastest thing in the universe. The event of horizon is the region in the blackhole where the escape velocity required is even higher than the speed of light, so even light cannot escape it once it enters the event of horizon (Tremaine, 2014). It is this area that gives the black holes this name as this part appears to be a black color hole as

shown in Figure 4. Since nothing is reflected back or emitted by the event of horizon it's very difficult to study what's happening inside it. All we can know is what's happening around it. The radius of this event horizon, which determines the size of a black hole, is called Schwarzschild radius as shown in Figure 5, and is directly proportional to the black hole mass (MBH):

$$R_{Sch} = \frac{2GM_{BH}}{C^2}$$

where G is the gravitational constant and c is the speed of light. Anything including light, when it passes by the event of horizon is captured by it due to its strong gravity. This also disturbs the space-time around it. Both these factors cause the light to bend through gravitational lensing. As a result, a dark zone is produced which is known as the event of horizon shadow (Zahid et al., 2023).
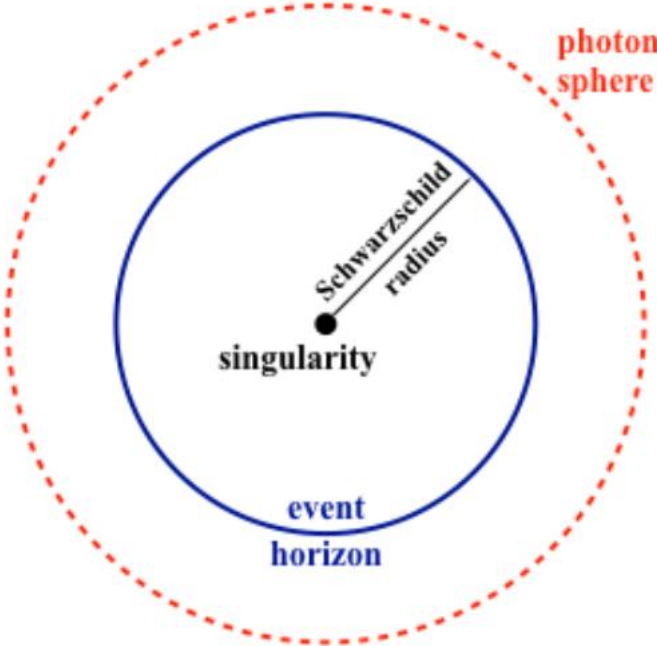
Figure 5: Anatomy of a Schwarzschild black hole.

2.3.2 Accretion disk

This is the disk around the event of horizon which is the main light source, and which makes blackholes visible to us as shown in Figure 3. The word accretion comes from a process in black holes where they take up surrounding matter to grow in size and mass (Tremaine, 2014). The consumed matter moves from the outer edge to the center of the black hole and eventually, it will fall into the event of the horizon and disappear. The accretion disk has different shapes depending upon the angle from where it is viewed because the light is bent due to the strong gravitational pull of the black hole through a process called gravitational lensing. There are two humps at the top and bottom as light is bending before it reaches us due to gravitational lensing. If viewed from above it appears to be an elliptical disk. It is geometrically thin but optically thick (Merloni et al., 2003).
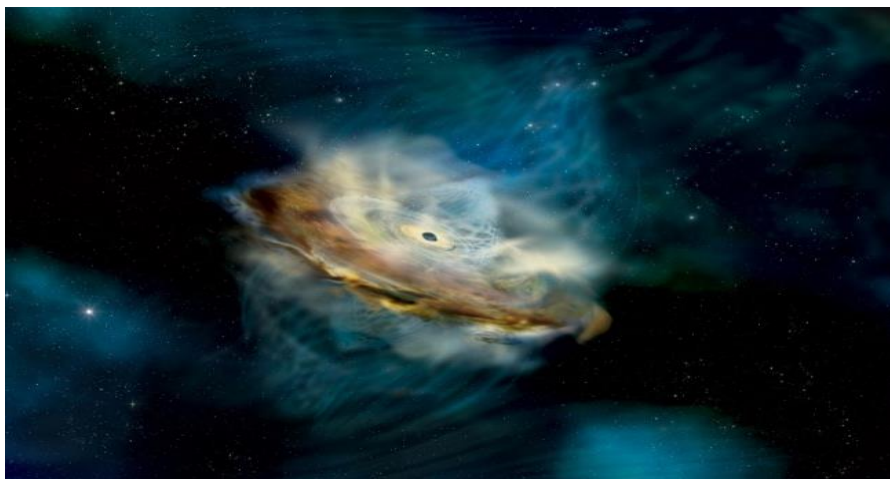
Figure 6: Photo showing an accreting black hole. Credit: NASA/Aurore Simonnet (Sonoma State University)

2.3.3 Photon sphere

Photon spheres are multiple rings of light around the black hole as shown in Figure 5. These rings are formed because light from the accretion disk revolves around the black hole numerous times before it reaches us. The rings that are closer to the black hole are thinner and fainter.

2.3.4 Doppler beaming

Doppler beaming is an effect observed in the accretion disk of a black hole similar to the Doppler effect of sound waves where waves fade away as the source moves away from the observer. A similar mechanism happens in black holes where the accretion disk when viewed from one angle appears brighter compared to the other side. This effect is felt due to the reason that the disk spins at a very high speed near the blackhole and light reaching us from the part of the accretion disk that is towards us appears to be bright and bluish while the light coming from the part of the disk that is spinning away from us appears to be less bright and reddish. The effect can be observed more prominently in the jets of the black hole.

2.3.5 Corona

Corona is believed to be one of the most extreme physical environments in the universe. Inside the accretion disk, there are magnetic field lines that extend from the inner part of the accretion disk to the outer region where these magnetic field lines create a region of highly unstable, rough, and hot matter that comes from the inner of a blackhole and extends outward similar to the corona of the sun. The matter in the corona is orbiting the black hole at a very high speed almost equal to the speed of light. Corona is a very good source of high-energy X-rays whereas X-rays coming from the inner accretion disk are a bit low in energy.

2.3.6 Particle jets

From the center of the black hole, highly energetic particles rush outwards forming jets of particles. These jets are formed because of the strong magnetic field lines in the accretion disk. These magnetic fields accelerate the charged particles in the accretion disk and these particles move along the magnetic field lines forming jets of charged particles along the axis of rotation of the black hole as shown in Figure 7.
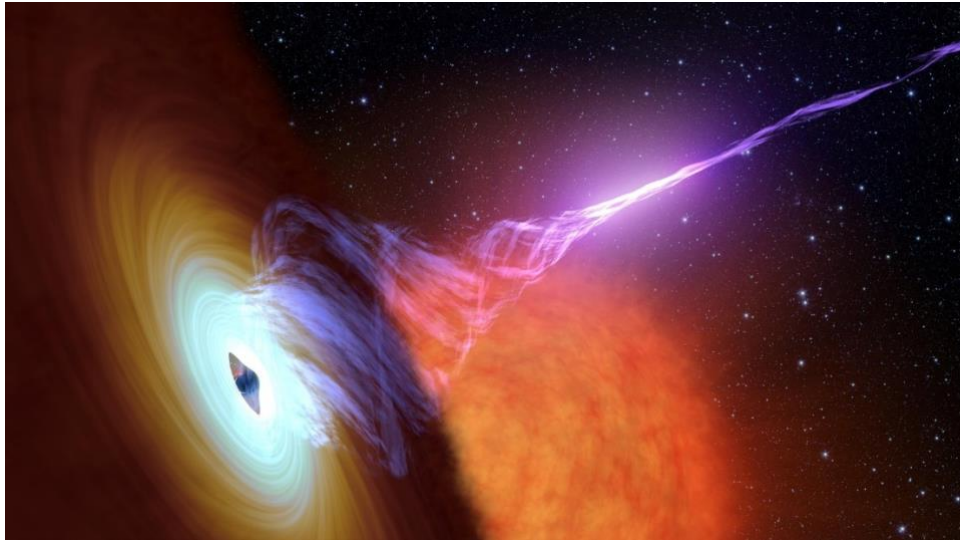
Figure 7: Photo of a Black hole with a jet of particles. Credits: NASA/JPL-Caltech

2.3.7 Singularity

According to the theory of general relativity, there is a point in the center of the black hole where gravity is so strong that all the matter is pressed to a point to have infinite density as shown in Figure 5. This is the end for anything that enters the event of horizon. Astronomers are still doing research about singularity as not much information is available about it.

2.4 Classification of black holes

Black holes can be divided into different categories based on different properties, but we use mass because it's the mass of a black hole that decides its gravitational strength and size. Here are different types of black holes based on their masses:
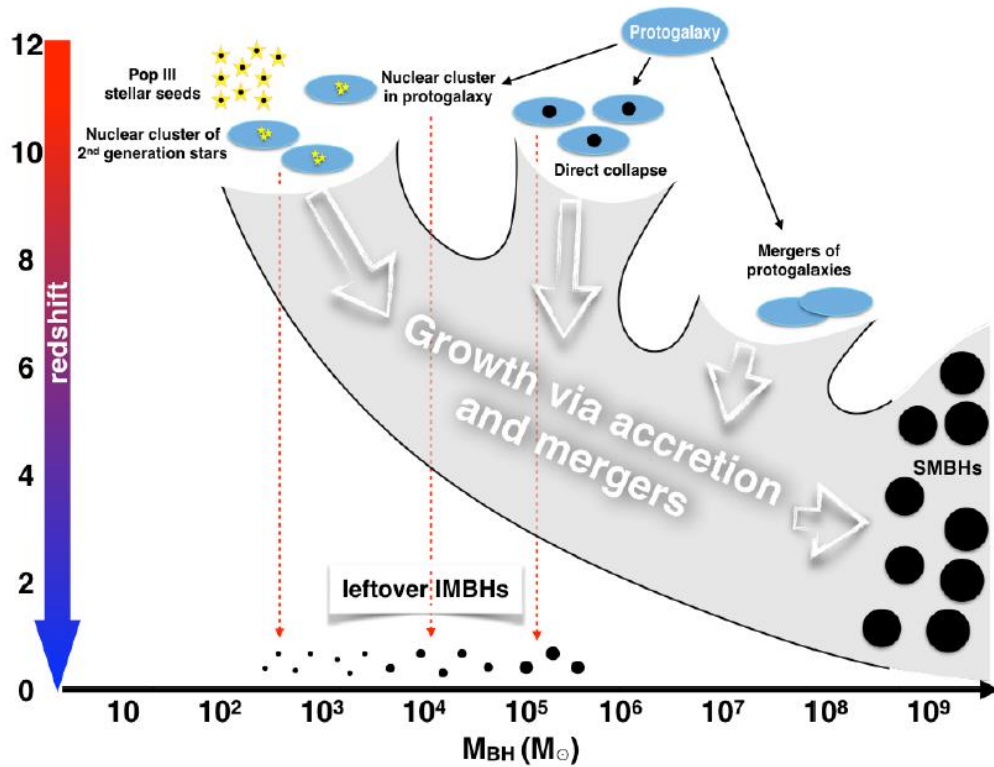
Figure 8: Seed BHs could form in the early Universe. These seeds are from Population III stars. Mergers in dense stellar clusters formed from either the second generation of stars or in flows in protogalaxies, or direct collapse of dense gas in protogalaxies, and grow to 10^9 $M_\odot$ by z=7. SMBHs could potentially arise directly by protogalaxies merging at z 6. Seed BHs that did not develop into SMBHs can be detected as remnant IMBHs in the local Universe.

2.4.1 Stellar mass blackholes

They are comparatively low-mass black holes with masses usually between a few times the solar mass to 100 times the solar mass (Cresci & Maiolino, 2018). As the name suggests these black holes are formed as the dense core of a star collapses after a supernova explosion. Stars have fuel in their core which is being used for nuclear reactions. After a certain time, all the fuel from the core of a star is used up and a supernova explosion happens after which black holes are formed. Theoretically, the mass of a stellar-mass black hole depends on the initial mass of the progenitor, how much mass is lost during the progenitor's evolution, and on the supernova explosion mechanism.

Stellar-mass black holes are formed from the collapse of massive stars (Casares & Jonker, 2014). Massive stars having mass greater than one solar mass usually having mass a few times the mass of the sun undergo a life cycle where they use the fuel in their core

for nuclear reactions. As a result of these nuclear reactions, a lot of pressure is produced that maintains the balance between inward gravitational force and outward pressure. Because of this balance between pressure and gravitational force, the star's structure is maintained. Towards the end of their lifetime when massive stars have consumed most of their fuel in the core, the core collapses under its own gravity and becomes tremendously dense and no outward pressure is there to balance the gravity. If the mass of the core surpasses a crucial threshold known as the Tolman-Oppenheimer-Volkoff (TOV) limit, the collapse continues until gravity becomes so severe that light cannot escape, resulting in the development of a black hole.

2.4.2 Intermediate mass black hole

These types of black holes fall between stellar-mass black holes and supermassive black holes. Although scientists are still working on the formation of Intermediate mass black holes (IMBH), it is thought that they are formed from the merging of smaller black holes or from the remnants of massive star clusters. There are clear and compelling cases for black holes in the mass range of 10^5 –10^6 M$_\odot$ in the nuclei of low-mass galaxies (Greene et al., 2020).

They are the link, thought to be missing for many decades, between stellar-mass and SMBHs and the possible seeds from which SMBHs in the early Universe grew. Finding proof of their existence is thus pivotal for understanding SMBH and galaxy growth (Mezcua, 2017) . In dense star clusters, such as globular clusters, the high density of stars can lead to frequent stellar collisions. Over time, these collisions can result in the formation of a more massive black hole in the center of the cluster. If enough stellar mass is accumulated, an IMBH could form through a series of mergers. In some scenarios, IMBHs could form through a series of merging processes. Stellar-mass black holes could merge to form intermediate-mass black holes, and these IMBHs could further merge to become supermassive black holes. This process could take place in the centers of galaxies. Just as massive stars can collapse into stellar-mass black holes, a supermassive cloud of gas could collapse directly into an IMBH (Johnson et al., 2011). This process would require very specific conditions, including a large amount of gas with minimal angular momentum.

2.4.3 Supermassive black holes

They are the most massive black holes discovered to date. Their masses fall between millions to billions of times the solar mass (Greene, 2012). These supermassive black holes (SMBH) are usually found in the center of most galaxies. Our galaxy's Milky Way also has supermassive black holes at its center known as Sagittarius A* (Zahid et al., 2023). Since they exist at the center of the galaxies it is thought that they are formed from the collapse of giant gaseous clouds in the galaxies, or they can also form from the merger of two or more small black holes. Active galactic nuclei, such as Seyfert galaxies and quasars, are powered by supermassive black holes. The largest supermassive black hole is in the galaxy cluster Abell 1201 and has a mass thirty billion times that of the Sun. One of the most widely accepted theories is that SMBHs form through the gradual accretion of gas and dust over long periods. As matter falls into a dense region at the center of a galaxy, it can accumulate and create a supermassive black hole.

Distant and early supermassive black holes, such as J0313–1806, and ULAS J1342+0928, are hard to explain so soon after the Big Bang. Some postulate they might come from the direct collapse of dark matter (Harada et al., 2017). DCBHs may be the seeds of the first supermassive black holes (SMBHs) because it is difficult for ordinary Population III (Pop III) star BHs to grow rapidly after birth. DCBHs are born with much larger masses and in much higher densities in host halos that can retain their fuel supply (Whalen et al., 2021). In the early universe, under the right conditions, a direct collapse of a massive cloud of gas could result in the formation of an SMBH without the intermediate formation of smaller black holes. The underlying notion revolves around a scenario where an exceptionally dense cloud of gas accumulates in a region of space. This accumulation can reach such density that it circumvents the typical process of giving rise to a protostar and going through nuclear fusion to become a main-sequence star. Instead, the gas cloud directly collapses under its own gravitational force, potentially bypassing several intermediate stages. The necessary conditions for the direct collapse of black holes are that the gas must be of a primordial composition and the gas should efficiently drop angular momentum and rapidly collapse avoiding fragmentation (Latif & Ferrara, 2016). This process would require pristine gas with minimal heavy elements. Another hypothesis is that SMBHs form through a series of mergers of smaller, intermediate-mass black holes

(IMBHs) as shown in Figure 8. Over time, these IMBHs would merge and grow into supermassive black holes. Scientists also predict that SMBHs may form by a combination of these processes.

2.4.4 Primordial black holes

Primordial black holes (PBH) have a lifetime equal to the age of the universe which means they were formed at the beginning of the universe after the Big Bang (Harada et al., 2017). It is thought that since after the Big Bang space was not uniform and there were areas with different densities, some with low density and others with high density and they may have been created from regions of high density (Martinelli et al., 2022).

One of the most widely studied mechanisms for PBH formation is the collapse of high-density regions in the early universe. Quantum fluctuations in the density of matter and radiation during the inflationary period of the universe can lead to local over-densities. If a region becomes sufficiently dense, it may undergo gravitational collapse to form a black hole (Harada et al., 2017).

2.5 Emissions associated with AGN

Accreting Direct Collapse Black Holes (DCBHs) are theoretical constructs, and there is an ongoing exploration of their characteristics. When matter accretes onto a black hole, whether it be a DCBH or another type, a range of emissions and processes can take place. As material descends into the gravitational field of the black hole, it undergoes heating due to friction and gravitational forces. This heated material emits X-rays, detectable by X-ray telescopes (Miller, 2007). These emissions serve as indicators of the extreme conditions proximate to the black hole. Geometrically thin and optically thick disc coupled with a hot corona produces X-ray emission (Merloni et al., 2003). Some of the material falling into the black hole can be propelled to exceedingly high speeds and energies. This acceleration can lead to the emission of gamma rays, the most energetic form of electromagnetic radiation. Gamma-ray emissions offer valuable insights into the processes transpiring in the vicinity of the black hole. The accretion disk encircling a black hole can emit radiation in the infrared and optical spectrums due to the elevated

temperatures of the matter within the disk. These emissions can offer insights into the structure and attributes of the accretion process.

2.6 Radio emission mechanisms of AGN

Radio waves are not emitted by black holes directly; rather, radio waves associated with black holes typically originate from their nearby surroundings. These sources can include the accretion disk, which consists of matter falling into the black hole, or from the high-speed particle jets ejected from the vicinity of the black hole. During active accretion events, wherein a black hole consumes nearby matter such as gas and particulate material from a companion star, an accretion disk is fashioned around the black hole. As this material undergoes a helical descent towards the event horizon, it undergoes elevation in temperature due to the effects of both friction and compression. This progression gives rise to the emission of remarkable thermal energy and radiation across the electromagnetic spectrum, encompassing radio wave frequencies. These radio waves arise from synchrotron radiation, an occurrence in which charged particles, predominantly electrons, execute helical trajectories along magnetic field lines at relativistic speeds, thereby generating radiation in the process. It is this synchrotron radiation that generates the radio emissions that are noticeable in the vicinity of black holes.

In certain instances, black holes accompanied by accretion disks have the capability to generate robust jets of particles that propel perpendicularly to the disk's plane. These jets have the potential to stretch across immense distances, emitting radiation across a spectrum of wavelengths, including radio frequencies. While the precise processes governing the generation and emission of these jets remain incompletely revealed, it is probable that they entail the influence of potent magnetic fields and the acceleration of charged particles to substantial speeds. The interplay between these particles and the magnetic fields is likely responsible for the phenomenon of synchrotron radiation, which gives rise to the radio emissions we detect (Miller, 2007). The observation of these radio emissions serves as a valuable instrument in the examination of black holes and the encompassing regions. Radio telescopes and instruments such as the Very Large Array (VLA), specialized in radio astronomy, have played pivotal roles in capturing imagery and data pertaining to accretion disks, jets, and the correlated radio emissions associated with

black holes. These observations provide valuable information regarding the dynamics, configuration, and material characteristics of black holes and their immediate surroundings.

Radio emission can originate from synchrotron emission from relativistic jets in radio-loud AGN while a wide range of mechanisms are involved in radio-quiet AGN, such as star formation, AGN-driven wind, free-free emission from photo-ionized gas, and innermost accretion disc coronal activity (Panessa et al., 2019). These mechanisms can produce radio emission at different scales, ranging from the host galaxy scale down to the innermost region near the SMBHs in radio-quiet AGN. The absence of luminous jets in radio-quiet AGN allows for the exploration of these various mechanisms with high precision and spatial resolution, thanks to the advancements in highly sensitive radio arrays.

Chapter 3: Radio Emission from Low Luminosity AGN

3.1 What are fundamental planes

Fundamental Planes (FP) are hypothetical planes that relate some specific properties of black holes in a fundamental way. While talking about AGN, fundamental planes of black holes are those planes that relate the mass of the black hole that is present at the center of an AGN to its x-ray and radio luminosity. The Fundamental Plane suggests that, at low-accretion rates, the physical processes regulating the conversion of an accretion flow into radiative energy could be universal across the entire black hole mass scale(Plotkin et al., 2012. The fundamental plane of black holes co-relates three important factors of blackholes that are the mass of the black hole, its X-ray luminosity, and Radio luminosity. According to (Merloni et al., 2003) radio luminosity of a BH depends on its X-ray luminosity and mass. Since the origin of radio and x-ray luminosity is the same that is both of them can be emitted by an accretion disk and the jets of black holes so they can be easily correlated (Merloni et al., 2003). In the past few years, fundamental planes have also been used to study the origin of X-rays being emitted by AGN (Plotkin et al., 2012).

The mass of an AGN defines its gravitational pull and the amount of matter that is being accreted onto the black hole. The greater the mass of an AGN, the greater its gravitational field. X-ray luminosity is the measure of X-rays radiated by the AGN in a unit of time. AGN emit radiation in a range of wavelengths which include low wavelength X-rays and high wavelength Radio waves. Since X-rays are being generated in the accretion disk of the black hole they are a great source of information about the accretion process. It also provides insight into the characteristics of the hot gas surrounding the black hole. Radio luminosity is the measure of radio waves emitted by the AGN in a unit of time. Radio waves are emitted due to many processes happening in AGN. These processes include interaction between the accreting matter and a strong magnetic field in the surroundings of a black hole. One of the most important forms of fundamental plane equation that describe the relationship between X-ray luminosity, Radio luminosity, and the mass of the black hole is given below:

$$\text{Log } L_R = \alpha \log L_X + \beta \log M_{BH} + \Upsilon \qquad (1)$$

Where L_R is the radio luminosity, L_X is the X-ray luminosity, M_{BH} is the mass of a black hole, and α,β, and ϒ are the coefficients that illustrate how these parameters are interrelated. These coefficients can have different values based on the sample of AGN that is under observation, or the observational technique being used. The Fundamental Plane equation also implies that low-luminosity black holes should be more and more radio-loud as the accretion rate decreases (Merloni et al., 2003). The relation was first seen in stellar-mass black holes, which have a narrow range in mass, and then extended to all black holes (Gültekin et al., 2014). The coefficient in the fundamental plane equation depends on sample selection and other physical parameters. Different coefficients are expected depending on the physical conditions and geometry very close to the black hole, and whether X-rays are dominated by optically thin jet synchrotron or not (Plotkin et al., 2012). Ideally, the largest possible dynamic range in mass and luminosity should be considered to obtain the most reliable FP coefficients. Understanding the fundamental plane equation helps astronomers understand the mechanism of accretion, energy emission, and matter ejection around black holes. It is also a very convenient way of calculating black hole masses and studying the evolution of AGN populations. In short, the fundamental plane of black holes is a key piece of equipment for astronomers to have an insight into the complex transition of matter and energy around supermassive black holes that are present at the center of AGN.

3.2 Calculating radio flux from the core of AGN

To develop a theoretical model that can compute Radio Emissions from low-mass AGN we calculate the Radio flux from DCBH at high redshift. We assume a black hole of mass 10^7 $M_\odot$ at redshift 10 accreting at Eddington accretion rate. To calculate the radio flux, the first step taken was to estimate their 5GHz Luminosity in the rest frame for which we needed X-ray Luminosity which was calculated using the bolometric luminosity equation from (Marconi et al., 2004) which is given as follows:

$$\text{Log} (L_{bol} / L_x) = 1.54 + 0.24 \,\mathscr{L} + 0.012 \,\mathscr{L}^2 - 0.0015 \,\mathscr{L}^3 \tag{2}$$

where $\mathscr{L} = \log L_{bol} - 12$ and L_{bol} is in units of solar luminosity.

The bolometric luminosity is given as:

$$L_{bol} = 1 \text{ x } L_{Edd} \tag{3}$$

Where,

$$L_{Edd} = \frac{4\pi G \, c \, mp \, M\odot}{\sigma_T} \left(\frac{M}{M\odot} \right) \tag{4}$$

Where, G = 6.67430×10−11 m³ kg⁻¹ s⁻² , m_p =1.6726219×10−27 kg, c = 299,792,458 m/s, $M_\odot$ = 1.989 x 10^{30} kg, σ_T = 6.65×10−29 m².

$$L_{Edd} = 1.26 \times 10^{38} \, (M_{BH} / M_\odot) \quad erg/s \tag{5}$$

So,

$$L_{Edd} = 1.26 \times 10^{45} \, erg/s \tag{6}$$

Converting Eddington Luminosity from erg/s to solar units.

1 solar unit = 3.846 x 10^{33} erg/s

So,

$$L_{Edd} = 3.27 \times 10^{11} \, L_o \tag{7}$$

And,

$$L_{bol} = 3.27 \times 10^{11} \, L_o \tag{8}$$

By substituting these values in equation (2) we get X-ray luminosity.

The X-ray luminosity calculated for a black hole with mass 10^7 $M_\odot$ accreting at Eddington accretion rate is 3.13 x 10^{41} erg/s. After calculating the X-ray luminosity, the next step was calculating the radio-luminosity. To do so we used different fundamental planes which are MER03 (Merloni et al., 2003), KOR06 (Körding et al., 2006), GUL09 (Gültekin et al., 2009), PLT12 (Plotkin et al., 2012) and BON13 (Bonchi et al., 2013), and substituted them in the given equation:

$$\text{Log } L_R = \alpha \log L_X + \beta \log M_{BH} + \Upsilon \tag{9}$$

Where the values of α, β, and ϒ are given in Table 1.

Table 1: Coefficients for different fundamental planes.

Fundamental Planes	α	β	Υ
MER03	0.60	0.78	7.33
KOR06	0.71	0.62	3.55
GUL09	0.67	0.78	4.80
PLT12	0.69	0.61	4.19
BON13	0.39	0.68	16.61

We added one more fundamental plane of equation 19 of (Gültekin et al., 2019) which has a slightly different form given as:

R = -0.62 + 0.70X + 0.74μ   (10)

Where,

$R = \log (L_R / 10^{38} \text{ erg/s})$ (11)

$X = \log (L_X / 10^{40} \text{ erg/s})$ (12)

$\mu = \log (M_{BH} / 10^{8} M_o)$ (13)

As we know, the radio flux is redshifted into a given band in the observer frame. The radio flux does not come from 5 GHz in the source frame, so we calculate it as follows:

$L_R = \upsilon L_\upsilon$ (14)

We assumed that the spectral luminosity L_υ is proportional to $\upsilon^{-\alpha}$ where α= 0.7.

The spectral luminosity in the rest frame is then used to calculate spectral flux in the observer frame using the following relation:

$$F_v = \frac{L_{v'}(1+z)}{4\pi d_L^2}$$ (15)

Where $\upsilon' = \upsilon (1+z)$ and d_L^2 is the luminosity distance which can be calculated using a cosmological calculator using Planck cosmological parameters given as $\Omega_M = 0.308$,

$\Omega_\Lambda = 0.691$, $\Omega_b h^2 = 0.0223$, $\sigma_8 = 0.816$, $h = 0.677$ and $n = 0.968$. Using all these steps we calculated the radio flux for a range of frequencies varying them from 0.1 GHz to 10 GHz. The calculated flux varies between 100 nJy and 2000 nJy for different fundamental planes.

3.3 Radio flux from HII regions

HII regions are interstellar spaces of ionized gas present in star-forming regions where hot and massive stars radiate ultraviolet radiations which are highly energetic. These energetic radiations remove electrons from hydrogen atoms in the surrounding areas causing them to form a region of positively charged ionized gas. This ionized region emits radiations at different wavelengths including large wavelength radio waves. Since free electrons are present in the vicinity of these positively charged hydrogen ions, these electrons approach the positively charged hydrogen ion but are deflected or accelerated by the electric field of the hydrogen ions and radiate radio waves. These radiations are called free-free or bremsstrahlung radiations.

Thermal bremsstrahlung in the HII region which are radiations emitted due to acceleration of a charge in Coulombs field of another charge can emit radio waves. To calculate radio flux from HII Regions we use the Photon Ionization rate Q_{Lyc} which is related to the star formation rate, so radio flux can be calculated as follows in Units of W/Hz:

$$L_v \leq \left(\frac{Q_{Lyc}}{63 \times 10^{52}}\right) \left[\frac{T_e}{10^4 k}\right]^{0.45} \left[\frac{v}{GHz}\right]^{-0.1} \tag{16}$$

Where, $Q_{Lyc} = $ SFR ($M_\odot$ yr^{-1})/ 1.0 x 10^{-53}. We assume $T_e = 10^4$ K (Condon et al., 1992). The flux calculated is in W/HZ we convert it to erg/s.Hz. Using the above-stated equation and conditions, luminosity is calculated which is further used in equation 13 to get radio flux for HII regions by varying frequency from 0.1 GHz to 10 GHz.

3.4 Radio flux from Supernova remnants

When a massive star reaches the end of its life cycle, it can undergo a cataclysmic explosion known as Supernova, releasing an immense amount of energy, and ejecting its outer layers into space. The core of the star collapses under the force of gravity, either forming a dense neutron star or collapsing further to become a black hole. The expanding

debris from the supernova explosion, consisting of gas and dust, creates a shockwave that propagates outward into the surrounding interstellar medium. This shockwave is responsible for heating and compressing the surrounding gas and dust, leading to the formation of a glowing, hot shell of material known as the supernova remnant. These remnants can persist for thousands to millions of years, gradually dissipating their energy and merging with the interstellar medium.

When a massive star explodes in a supernova, it creates a powerful shockwave that rapidly expands into space, pushing out the outer layers of the star. As this shockwave moves through the interstellar medium, it compresses and heats the surrounding gas and magnetic fields. Within the shockwave, there are magnetic fields that can accelerate charged particles, particularly electrons, to extremely high energies. These electrons gain kinetic energy as they interact with the shockwave's magnetic fields. These high-energy electrons spiral along the magnetic field lines within the SNR. As they spiral, they emit synchrotron radiation in the form of radio waves. This emission is a consequence of the charged particles' acceleration and the deflection caused by the magnetic field. To calculate radio flux from supernova remnants we use equation 21 of (Condon et al., 1992):

$$\frac{L_v}{W/Hz} \sim 5.3 \; x \; 10 \left[\frac{v}{GHz}\right]^{-\alpha} \left[\frac{SFR(M \geq 5M\theta)}{M \; yr}\right] \tag{17}$$

Where α = 0.8. The luminosity calculated by this equation is used in equation 13 to get radio flux from supernova remnants by varying frequency from 0.1 GHz to 10 GHz.

3.5 Radio flux from Jets

Launching the jet relies on the presence of a very strong magnetic field close to the black hole's surface. It is found that indeed the magnetic field amplification mechanism works during the accretion process around a DCBH (Latif et al., 2014). During the formation of the SMBH, it rapidly accretes mass from the collapsing super massive star and launches very energetic jets that might unbind most of the gas in the galaxy (Bear & Soker, 2020). To estimate the radio flux from the jets of BHs we first estimate their jet power. To do so we follow the same method as followed by (Yue & Ferrara, 2021). The relation between the jet power, black hole mass, spin, and magnetic flux is:

$$P\text{jet} = \frac{k}{4\pi c} \; \Phi^2_{\text{BH}} \;\; \Omega^2_{\text{H}} \;\; f(\Omega_{\text{H}}) \tag{18}$$

Where, $f = 1 + 1.38 \, (\Omega_{\text{H}} \, r_{\text{g}} \,/c \,)^2 - 9.2 \, (\Omega_{\text{H}} \, r_{\text{g}} \,/c \,)^4$, $\kappa = 0.05$ is the numerical coefficient which depends weakly on the magnetic field geometry , $\Omega_{\text{H}} = ac/2r_{\text{H}}$ is the angular frequency, $r_{\text{H}} = r_{\text{g}} \, [1 + (1-a^2)^{1/2}]$ is the radius of Horizon, $r_{\text{g}} = GM_{\text{BH}} /c^2$ is the gravitational radius of the black hole, $a = Jc/GM^2_{\text{BH}}$ is a dimension less spin parameter, $\Phi_{\text{BH}} = 50 \, (\dot{M}_{\text{BH}} \, r^2_{\text{g}} \, c)^{1/2}$ is the limiting magnetic flux, and $\dot{M}_{\text{BH}} \, c^2 = 1.26 \times 10^{38} \, M_{\text{BH}}$

$(1-\varepsilon)/\varepsilon$ erg/s.

Substituting all these equations in equation 18 yields that a black hole with mass $10^7 \, M_\odot$ accretion at Eddington accretion rate with a spin parameter of 0.4 will have a jet power of 10^{45} erg/s.

To calculate the flux from the jets we use the empirical equation relating jet power with radio power. We use equation 1 of (Yue & Ferrara, 2021) which gives radio luminosity at 1.4GHz. the equation is given below:

$$\log\left[\frac{P_{jet}}{10^{42} erg/s}\right] = \rho_0 \log\left[\frac{L_{1\cdot4}}{10^{24} W/Hz}\right] + \rho_1 \tag{19}$$

Where, $L_{1.4}$ is radio luminosity at 1.4 GHz, $\rho_0 = 0.35$, $\rho_1 = 1.85$ and P_{jet} is the jet power of the accreting BH.

Substituting these values in equation 19 we can estimate the radio luminosity at 1.4 GHz. As we know, the radio flux is redshifted into a given band in the observer frame. The radio flux does not come from 5 GHz in the source frame, so we calculate it as follows:

$$L_R = \upsilon \, L_\upsilon \tag{14}$$

We assumed that the spectral luminosity L_υ is proportional to $\upsilon^{-\alpha}$ where $\alpha = 0.7$.

The spectral luminosity in the rest frame is then used to calculate spectral flux in the observer frame using the following relation:

$$F_\upsilon = \frac{L_{\upsilon'}(1+z)}{4\pi d_L^2} \tag{15}$$

Where $\upsilon' = \upsilon(1+z)$ and d_L^2 is the luminosity distance which can be calculated using a cosmological calculator using Planck cosmological parameters given as $\Omega_M = 0.308$,

$\Omega_\Lambda = 0.691$, $\Omega_b h^2 = 0.0223$, $\sigma_8 = 0.816$, $h = 0.677$ and $n = 0.968$. Using all these steps we calculated the radio flux for a range of frequencies varying from 0.1 GHz to 10 GHz.

Chapter 4: Results and Conclusions

4.1 Comparison with previous work

In order to validate the results of our theoretical model, we conducted an empirical analysis on CR7 and generated results for it. We used Figure 1 in (Whalen et al., 2020) as our benchmark and compared our results to it. Figure 9 below shows the results for CR7 generated by our theoretical model which are consistent with Figure 1 of (Whalen et al., 2020). Here we have used the data for CR7 i-e a DCBH with a mass of 4.4 x 10^6 $M_\odot$ accretion at 40% Eddington accretion rate at redshift 6.6 and applied telescope limits for ngVLA and SKA for over a 24-hour integration period, as previously detailed in the aforementioned paper. Figure 9 also shows the radio flux for HII regions with a Star formation rate (SFR) of 50 ($M_\odot$ yr^{-1}) shown by a dashed green line.

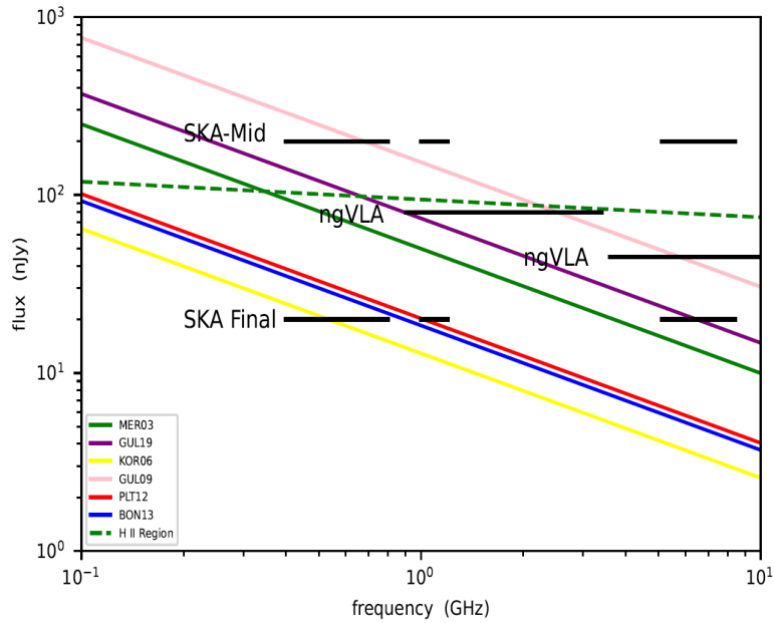Figure 9: Radio flux for different fundamental planes at z= 6.6. Black hole mass 4.4 x 10^6 $M_\odot$, Accretion rate = 0.4 x L_{Edd}, and spectral index α=0.7. The dashed line shows flux for HII regions with SFR = 50 ($M_\odot$ yr^{-1}).

4.2 Bolometric, radio, and x-ray luminosity for different accretion rates

In this study, we investigated the influence of black hole mass and accretion rates on bolometric luminosity, X-ray luminosity, and radio luminosity, focusing on a range of black hole masses commonly associated with supermassive DCBHs. Our analysis is conducted using three distinct accretion rate regimes: sub-Eddington, Eddington, and super-Eddington. Using equation 3 we generated the data for bolometric luminosity for different accretion rates and different black hole masses. We observe that bolometric luminosity exhibits a direct proportionality with black hole mass, which aligns with theoretical expectations. Additionally, higher accretion rates lead to increased bolometric luminosity. Our calculations indicate that bolometric luminosity spans a range from 10^{40} erg/s and 10^{46} erg/s for black hole masses varying from 10^4 to 10^7 $M_\odot$. The generated data has been visually represented in Figure 10.

We used Equation 2 to generate the data for X-ray luminosity. Similar to bolometric luminosity, X-ray luminosity displays a positive correlation with black hole mass, with larger black holes emitting more X-rays. Furthermore, higher accretion rates result in elevated X-ray luminosity. Our analysis suggests that X-ray luminosity can be anticipated to vary from 10^{39} erg/s to 10^{42} erg/s over the range of black hole masses from 10^4 to 10^7 $M_\odot$. Figure 11 represents the data for X-ray luminosity. Using equation 7 and the fundamental plane equation of Merloni et al. (2003) we generated data for radio luminosity by varying black hole mass and Eddington accretion rates. Radio luminosity also shows a direct relationship with black hole mass and accretion rates. Our data suggests that, according to the fundamental plane equation of Merloni et al. (2003), radio luminosity is projected to range between 10^{34} erg/s and 10^{36} erg/s for black hole masses within the 10^4 to 10^7 $M_\odot$ range, with luminosity increasing as both black hole mass and accretion rate rise. Figure 12 shows the radio luminosity of black hole mass ranging from 10^4 to 10^7 $M_\odot$ accreting at sub-Eddington, Eddington, and super-Eddington accretion rates.
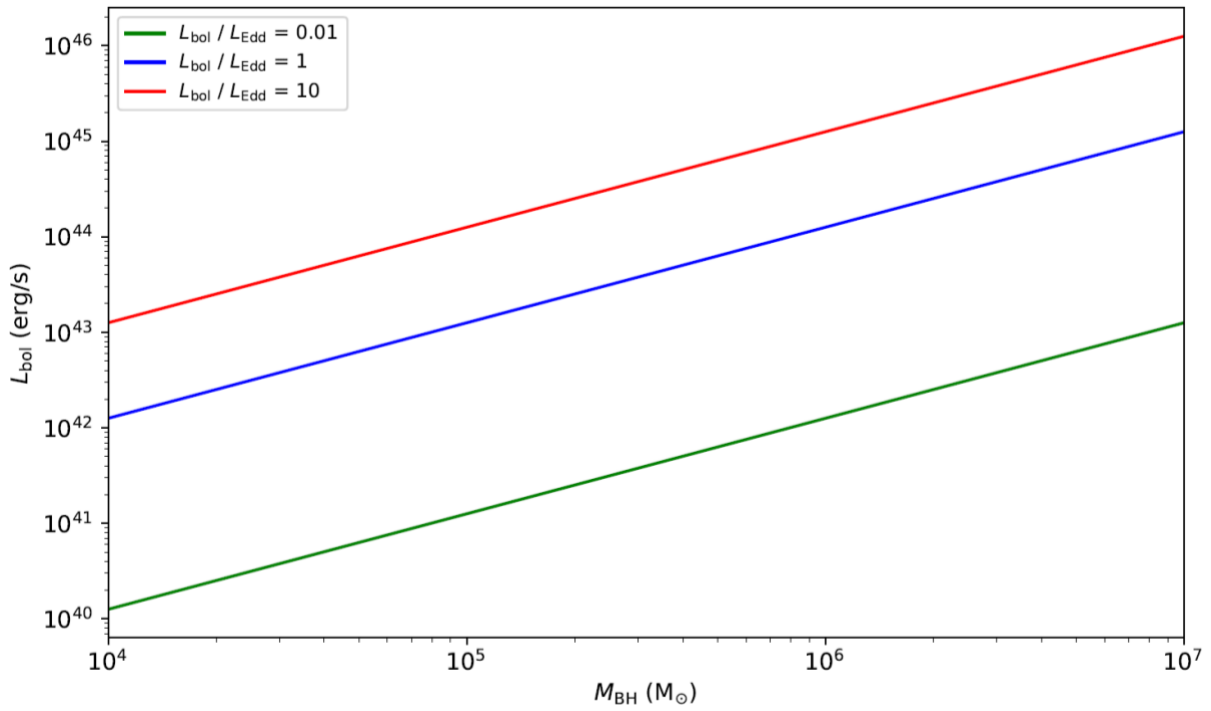
Figure 10: Bolometric Luminosity for different blackhole masses. Flux is shown at different accretion rates.
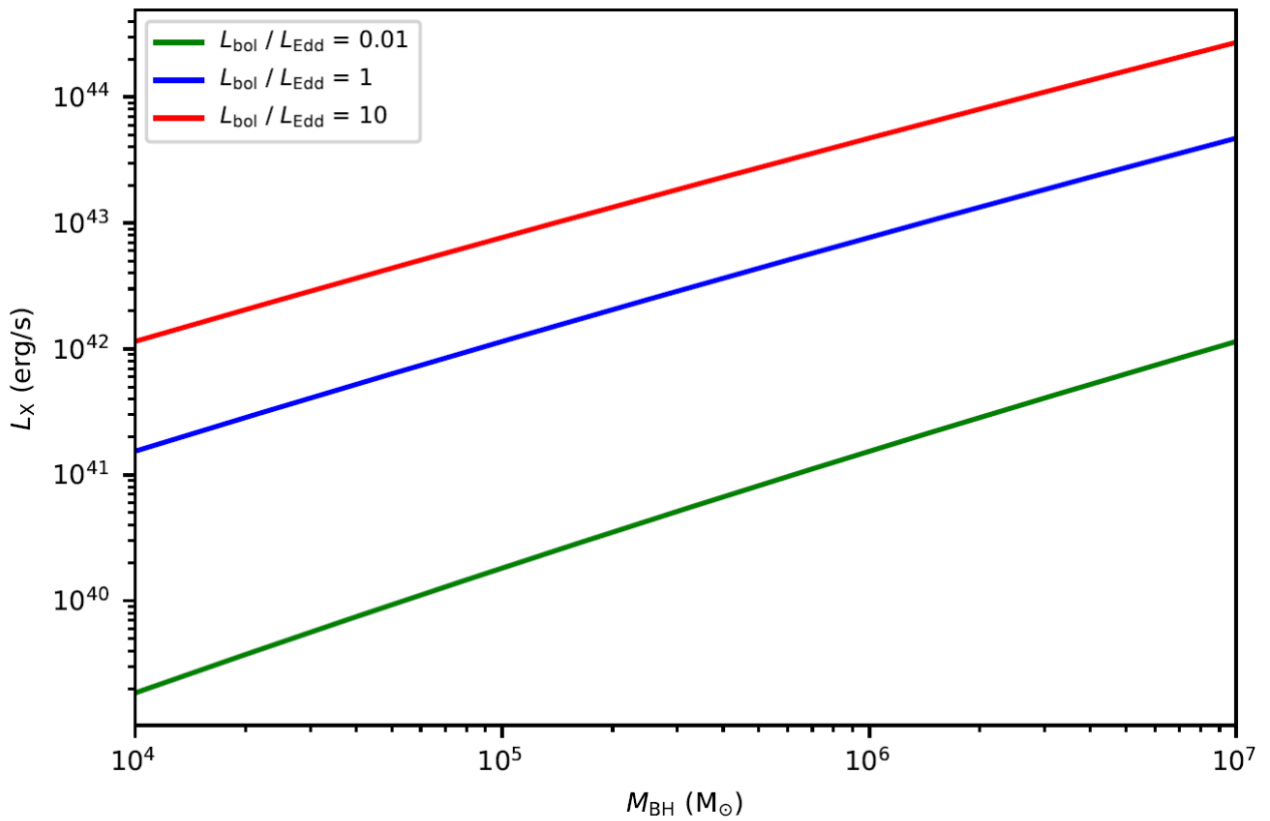

Figure 11: X-ray Luminosity for different blackhole masses. Flux is shown at different accretion rates
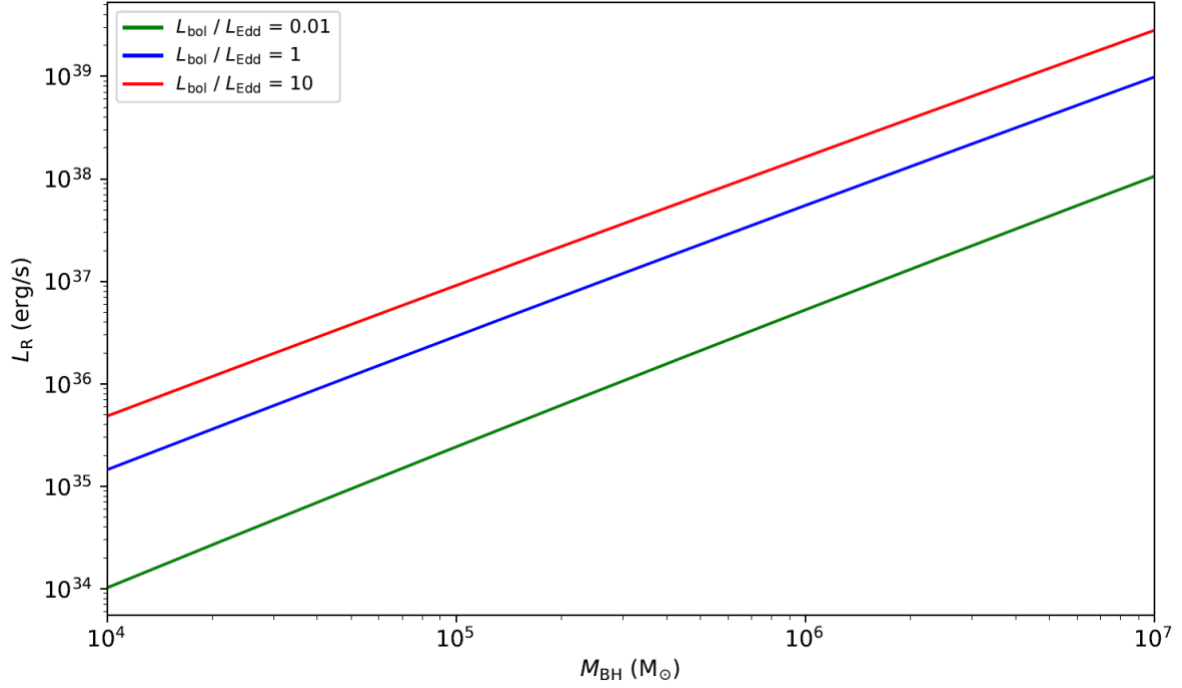
Figure 12: Radio Luminosity for different blackhole masses. Flux is shown at different accretion rates using the fundamental plane equation of (Merloni et al., 2003)

4.3 Radio flux from BH for different fundamental planes

Applying Equation 13, we systematically varied the frequency range from 0.1 GHz to 10 GHz in order to analyze the flux over six different fundamental planes. The black hole masses that we studied were 10^5, 10^6, and 10^7 solar masses, all of which were located at a redshift of 10 and were accreting at the Eddington accretion rate. Using our theoretical model, we then produced data, which we then displayed in Figure 13. In order to provide more context for our findings, we plotted the telescope limitations for various integration times, as shown in Tables 2 and 3, for the Next-Generation Very Large Array (ngVLA) and the Square Kilometer Array (SKA). The idea was to use these upcoming telescopes to determine whether black hole masses are observable.

Across all fundamental plane equations, our investigation showed an interesting trend, the flux showed an inverse relationship with frequency. Additionally, the results highlighted the fact that larger black holes produced higher flux, indicating that an increase in black hole mass was accompanied by an increase in the measured flux. Therefore, Figure 13 not only summarizes these empirical findings but also functions as a forecasting tool to evaluate SKA and ngVLA's observational capacities. Crucially, our figure

illustrates that black holes with masses smaller than $10^7 \, M_\odot$ are outside the observational capabilities of both ngVLA and SKA. It is nevertheless important to highlight that, when taking into account black holes with a mass of $10^7 \, M_\odot$, given an integration time of 100 hours, some fundamental planes, like those suggested by (Gültekin et al., 2019; Gültekin et al., 2009; Merloni et al., 2003), show promise for observation. It is important to recognize that these predictions depend on several characteristics, such as black hole masses, redshift values, accretion rates, and the selection of fundamental planes. These parameters have been studied in our theoretical model and the results are shown in upcoming sections.

Table 2: Telescope limits for SKA for different integration times.

Telescope limits for SKA for different integration times				
Frequency range (GHz)	0.1-0.3	0.3-1.05	0.95-1.76	5.8-10
Radio Flux (nJy) 1 hour integration time	14000	4400	2000	1300
Radio Flux (nJy) 10-hour integration time	4400	1391	632	411
Radio Flux (nJy) 100-hour integration time	1200	440	200	130

Table 3: Telescope limits for ngVLA for different integration times (Plotkin & Reines, 2018).

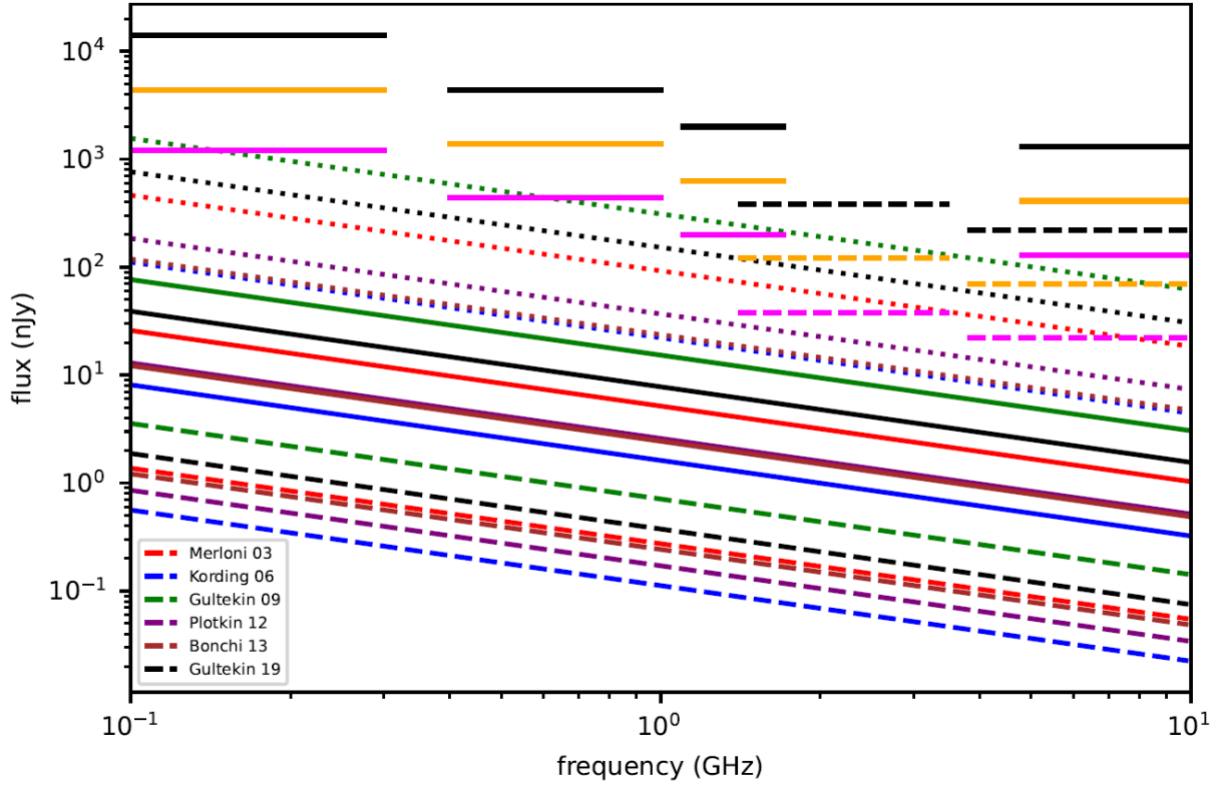| Telescope limits for ngVLA for different integration time		
Frequency range (GHz)	1.2-3.5	3.6-10
Radio Flux (nJy) 1 hour integration time	382	220
Radio Flux (nJy) 10-hour integration time	121	70
Radio Flux (nJy) 100-hour integration time	38	22

Figure 13: Radio flux for different fundamental planes at z= 10. Flux is shown at accretion rate = 1 x L_{Edd}, and spectral index α=0.7. The dashed line shows flux for blackhole mass 10^5 $M_\odot$, the solid line shows flux for blackhole mass 10^6 $M_\odot$ and the dotted line shows flux for blackhole mass 10^7 M. Telescope limits are also shown in the Figure 12 where pink lines show telescope limits for SKA and ngVLA for integration time 100 hours, orange lines for integration time 10 hours and black lines for integration time 1 hour. Dashed lines show limits for ngVLA while solid lines are for SKA.

4.4 Radio flux for BH for different fundamental planes by varying redshifts

Using equation 13 we also calculated flux for six different fundamental planes by varying redshift from 6 to 20, for different black hole masses of 10^5,10^6 and 10^7 $M_\odot$. This is the redshift range predicted by some theories to have the maximum comoving number density of DCBHs (Valiante et al., 2017). We plotted data for four different frequencies that are 500 MHz, 1.5 GHz, 6.5 GHz, and 12.5 GHz in Figure 6. Figure 14 suggests that flux increases when redshift decreases which is obvious as closer objects will have a higher flux. Tables 4 and 5 have telescope limits for SKA and ngVLA for different integration times at different frequencies.

Since flux at lower frequencies is higher, it is clear that flux at 1.5 GHz can be easily observed by telescopes compared to 6.5 GHz and 12.5 GHz. Figure 14 shows that ngVLA at 1.5 GHz and 6.5 GHz with 100-hour integration can observe a few fundamental planes at lower redshifts. The Figure 14 clearly shows that the radio flux of (Gültekin et al., 2019) can be observed for all redshifts from 20-6 at 1.5 GHz and 6.5 GHz with ngVLA with 100-hour integration time.

Table 4: Telescope limits for SKA for different integration times.

Telescope limits for SKA for different integration time				
Frequency range	500 MHz	1.5 GHz	6.5 GHz	12.5 GHz
Radio Flux (nJy) 1 hr integration time	4400	2000	1300	1200
Radio Flux (nJy) 10 hr integration time	1391	632	411	379
Radio Flux (nJy) 100 hr integration time	440	200	130	120

Table 5: Telescope limits for ngVLA for different integration times (Plotkin & Reines, 2018).

Telescope limits for ngVLA for different integration time				
Frequency range	500 MHz	1.5 GHz	6.5 GHz	12.5 GHz
Radio Flux (nJy) 1 hr integration time	-	382	220	220
Radio Flux (nJy) 10 hr integration time	-	121	70	70
Radio Flux (nJy) 100 hr integration time	-	38	22	22
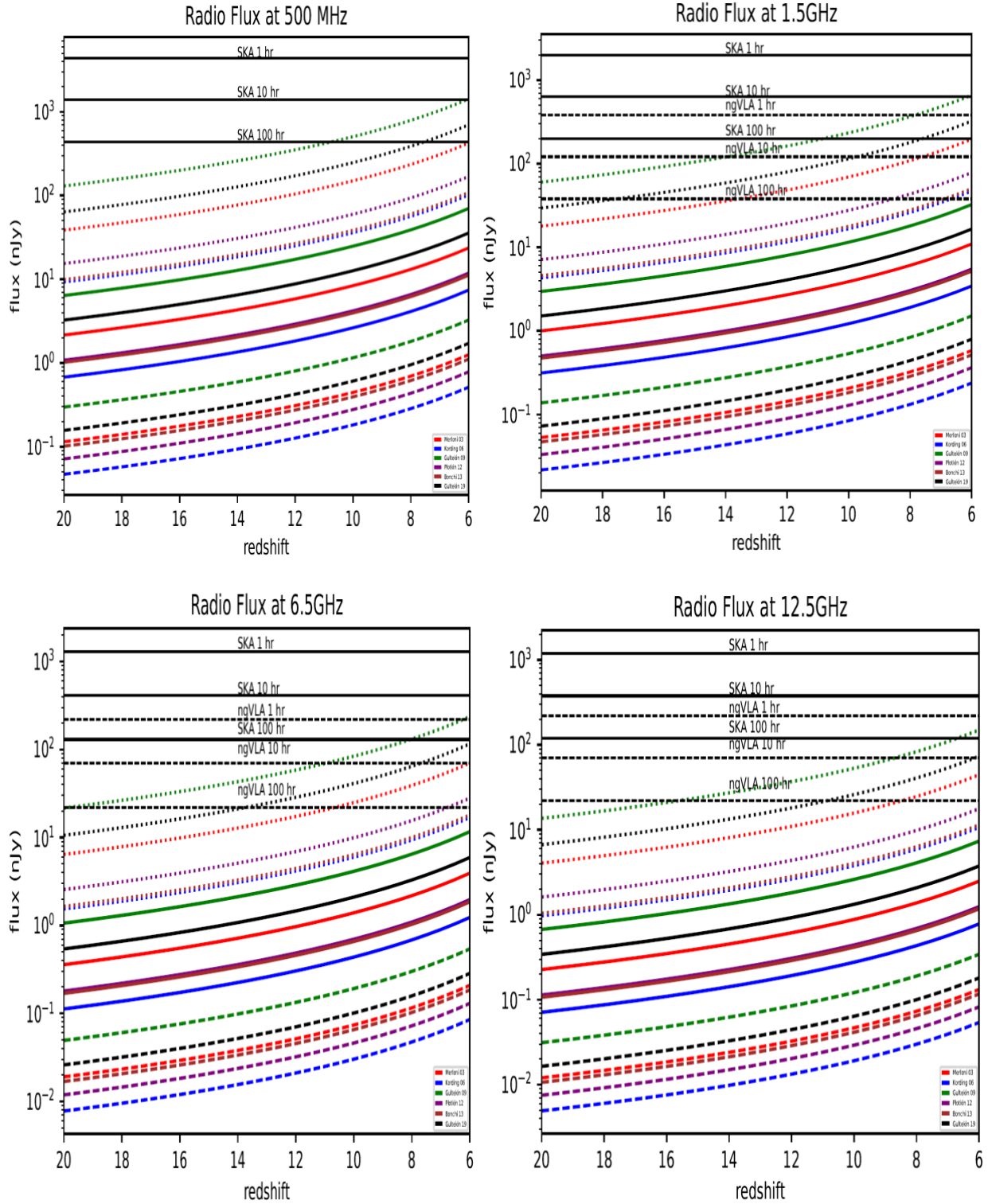
Figure 14: Radio flux at different redshifts. Flux is shown for different frequencies, Accretion rate = 1 x L_{Edd}, and spectral index α=0.7. The dashed line shows flux for blackhole mass 10^5 M⊙, the solid line shows flux for blackhole mass 10^6 M⊙ and the dotted line shows flux for blackhole mass 10^7 M⊙. The top left figure is for flux at 500 MHz, the top right for flux at 1.5 GHz, the bottom left for flux at 6.5 GHz, and the bottom right for flux at 12.5 GHz. The solid black lines show the telescope limits for SKA and the dashed black lines show telescope limits for ngVLA.

4.5 Radio flux for different spectral indices

The spectral energy distribution (SED) properties of the radiation are linked to our understanding of numerous physical mechanisms that produce cosmic radio emission. Radio SEDs can be defined by a power law and are often smooth (De Gasperin et al., 2018). Thus, a crucial variable known as the spectral index can be defined as the radio SED slope measured in a log-log plane. When ν is a negative number, the spectrum index (α) for a frequency and flux density S_v is given by:

$$S_v \propto \nu^{\alpha}$$

Radio SEDs often decrease with increasing frequency. This resulted in the opposite sign convention for α ($S_v \propto \nu^{-\alpha}$). Using equation 13 we also calculated flux for six different fundamental planes by varying frequency from 0.1 to 10 GHz, for different black hole masses of $10^5, 10^6$ and 10^7 M$_\odot$. We plotted data for two different spectral indices 0.7 and 0.3 which are suggested by observation data. The plot in Figure 15 clearly suggests that flux is higher at 0.7 compared to 0.3 spectral index. For the fundamental plane of (Merloni et al., 2003) the flux for spectral index 0.7 is 450 nJy which changes to 250 nJy when the spectral index is 0.3.
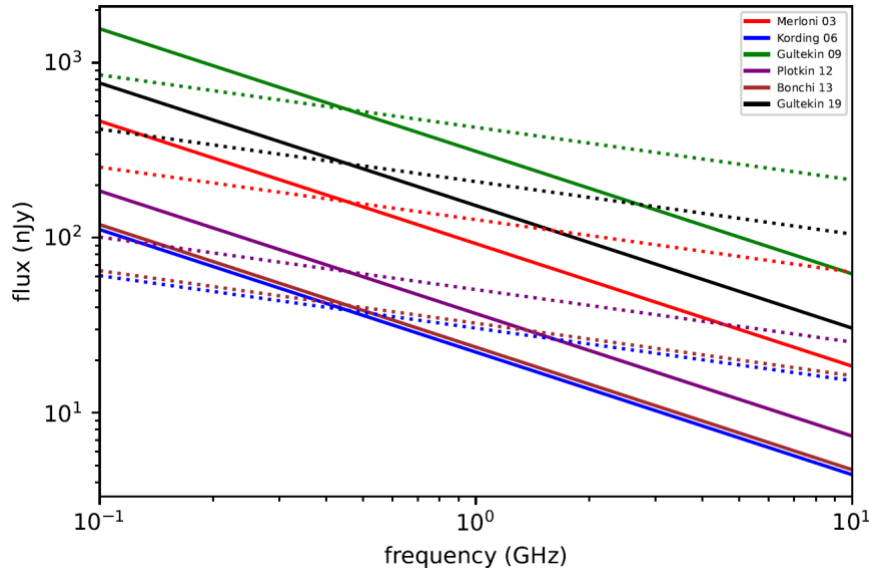

Figure 15: Radio flux for two different spectral indices. Flux is shown at redshift z=10, Accretion rate = 1xLedd, and blackhole mass 10^7 M$_\odot$. The solid line is for spectral index 0.7 and the dotted line is for spectral index 0.3.

4.6 Radio flux for BH at different Eddington accretion rates

We also estimated the dependence of flux on the accretion rate of DCBH. To do so we used the same method as described in Chapter 3 to calculate the flux by varying Eddington accretion rates from sub-Eddington accretion rates (that is less than 1%) to super-Eddington accretion rates (that is greater than 100%). The data collected is plotted in Figure 16 which suggests that the greater the Eddington accretion rate greater will be the flux generated by DCBH.

We also plotted the telescope limits to predict which accretion rates can be observed with upcoming telescopes for different integration times. The plot suggests that a black hole with mass 10^7 M$_\odot$ accreting at super-Eddington accretion rate can be easily observed with ngVLA 100-hour integration time for almost all the fundamental planes except Bonchi et al. (2013).
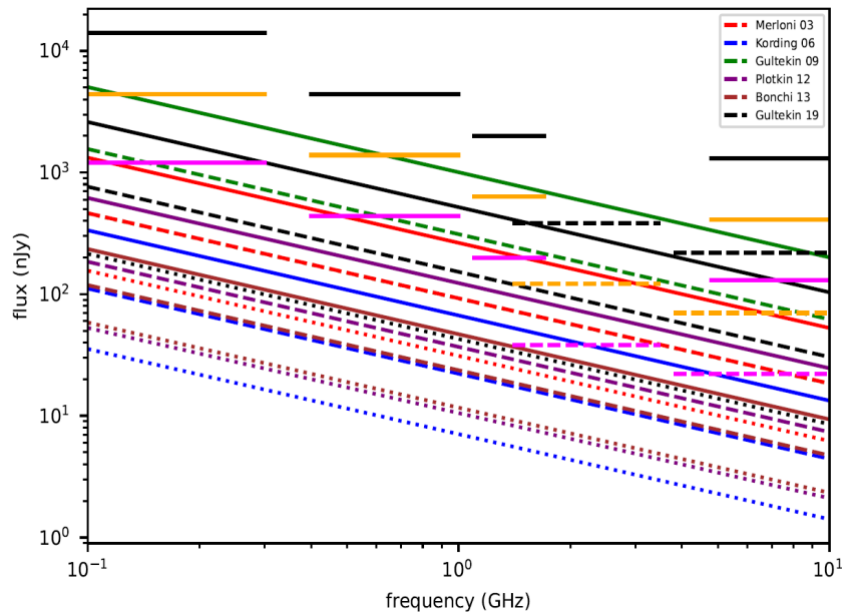
Figure 16: Radio flux at different accretion rates. Flux is shown for spectral index α=0.7, blackhole mass=10^7 M$_\odot$, and redshift=10. The dashed line shows flux for Accretion rate = 1 x L$_{Edd}$, the solid line shows flux for Accretion rate = 10 x L$_{Edd}$, and the dotted line shows flux for Accretion rate = 0.1 x L$_{Edd}$. Telescope limits are also shown in the figure where pink lines show telescope limits for SKA and ngVLA for an integration time of 100 hours, orange lines for an integration time of 10 hours, and black lines for an integration time of 1 hour. Dashed lines show limits for ngVLA while solid lines are for SKA.

4.7 Radio flux from the jet of the BH

Using equation 18 we estimate the jet power for different black holes with masses 10^5, 10^6, and 10^7 M$_\odot$ which turn out to be jet power of 10^{43} erg/s, 10^{44} erg/s, and 10^{45} erg/s respectively. Using these jet powers in equation 19 we estimated the jet flux for BHs with the previously mentioned masses at redshift 10. Our estimates predict the flux to be in the range of 35 to 10^7 nJy for a range of BH mass. Figure 17 shows that jet flux increases with a factor of 10^3 with black hole mass increasing by a factor of 10 which is clearly consistent with equation 19. Jet power depends on other factors as well like spin parameter, accretion rate, and redshift but currently, we just studied the effect of BH mass. Figure 17 also suggests that jet flux varies inversely with frequency as it has a high value for lower frequencies and lower values for higher frequencies.
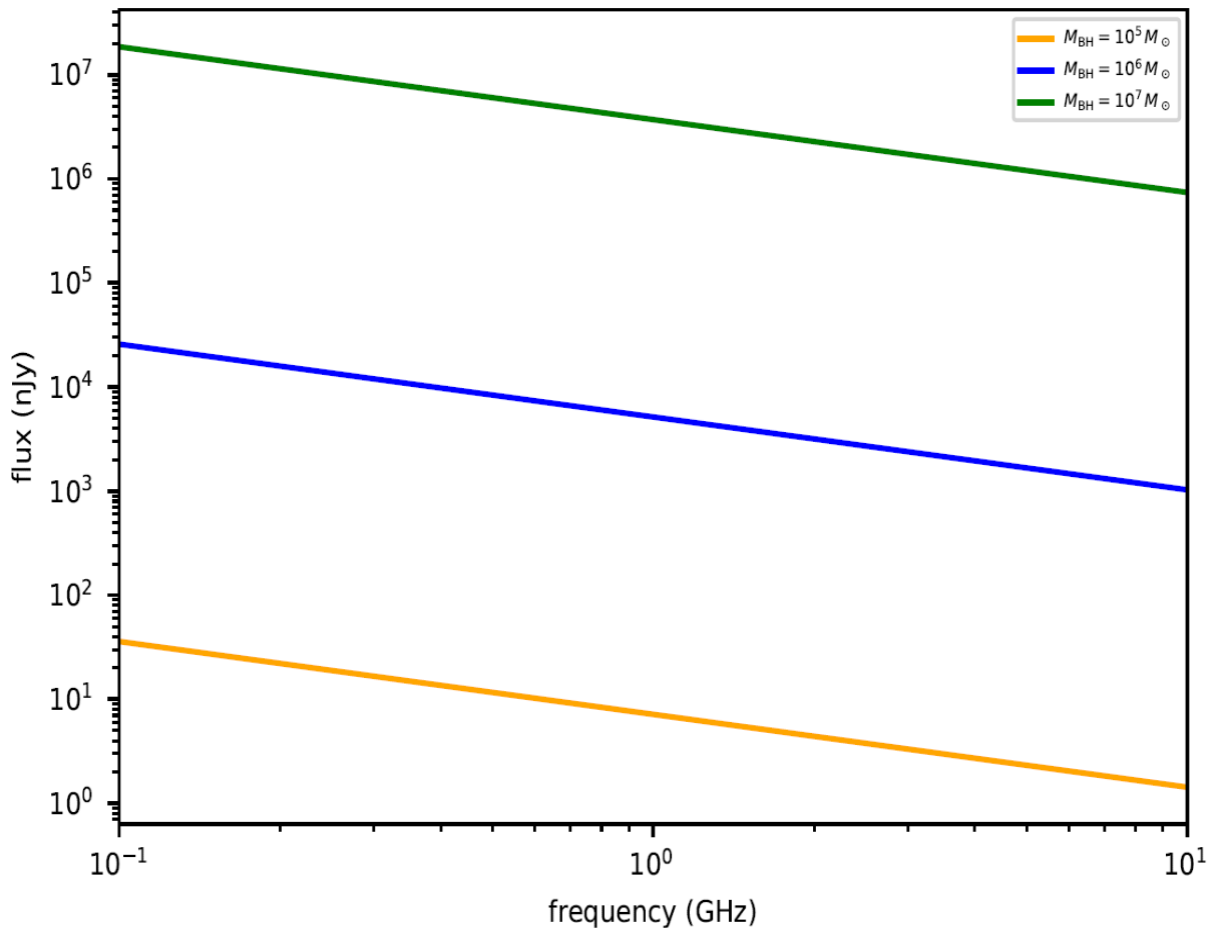

Figure 17: Jet flux for different black hole masses. Flux is shown at redshift 10 and spin parameter 0.4 for a range of frequency varying from 0.1 to 10 GHZ.

4.8 Radio flux from six fundamental planes, Supernova Remnants, HII regions, and Jet with telescope limits to predict observable radio flux

Using equations 14 and 15 we calculated the radio flux from HII regions and Supernova remnants respectively for SFR of 1 $M_\odot$ yr^{-1} and plotted the data in Figure 18 along with the flux from the core and jets of DCBH. The plot clearly shows that the radio flux from DCBH can be clearly differentiated from the flux from HII regions and Supernova remnants as flux for HII regions is low that is a few nJy while the flux from six fundamental planes ranges between 100 nJy and 2000 nJy. The flux from HII regions varies slightly with frequency while the flux from Supernova remnants varies inversely with the frequency.

Putting the telescope limits suggests that ngVLA with a 100-hour integration time can observe the flux from a few fundamental planes while SKA can hardly predict anything even at a 100-hour integration time. Flux from HII regions and supernova remnants cannot be observed with either ngVLA or SKA. Increasing the integration time can give us a better understanding of the flux from these sources.
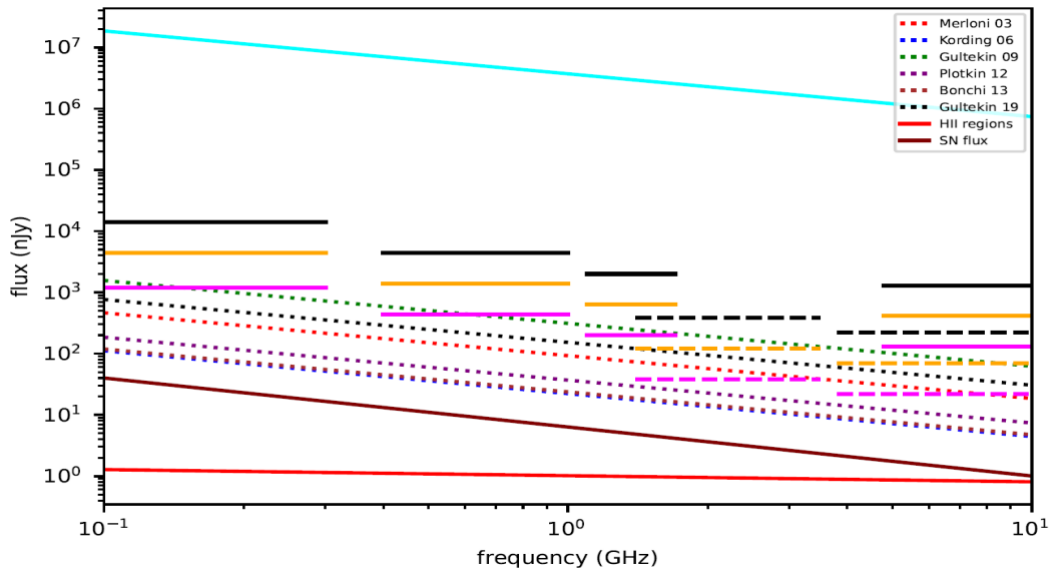
Figure 18: Radio flux for different fundamental planes. Flux is shown at black hole mass 10^7 $M_\odot$, Accretion rate = 1 x L_{Edd}, and spectral index $\alpha = 0.7$. Telescope limits are also shown in the figure where pink lines show telescope limits for SKA and ngVLA for an integration time of 100 hours, orange lines for an integration time of 10 hours, and black lines for an integration time of 1 hour. Dashed lines show limits for ngVLA while solid lines are for SKA.

4.9 Predictions for recently observed galaxies by JWST

We applied our theoretical model to the newly observed galaxies by JWST to make predictions for upcoming telescopes SKA and ngVLA for different integration times. The data collected from JWST for different sources is shown in Table 6 (Scoggins & Haiman, 2023; Maiolino et al., 2023). Using the data from Table 6 we generated data for these sources which are plotted in Figure 19. We predicted radio flux from the core for these sources using the six fundamental plane equations. Since SFR for these galaxies are not available yet we couldn't predict the radio flux from HII regions and Supernova remnants. Table 7 and 8 shows the possibility of the detection of these galaxies by SKA and ngVLA in the future. It can be clearly seen in Figure 19 that some of these galaxies can be observed by SKA and ngVLA with different integration times after the launch of these telescopes.

Table 6: Data for newly observed galaxies by JWST.

Source ID	Redshift z	Log (M_{BH}) ($M_\odot$)	L/L_{edd}	Log L_{bol} (erg/s)
10013704	5.919	5.65	1.06	43.8
8083	4.6482	7.25	0.16	44.6
3608	5.268	6.82	0.11	44.0
11836	4.409	7.13	0.2	44.5
20621	4.681	7.3	0.18	44.7
73488	4.1332	7.71	0.16	45.0
77652	5.229	6.86	0.38	44.5
61888	5.874	7.22	0.32	44.8
62309	5.172	6.56	0.39	44.2
53757	4.4480	7.69	0.05	44.4
954	6.760	7.9	0.42	45.6
GN-z11	10.6	6.2	5.5	45.0
UHZ1	10.3	7.602	1	45.7
CEERS 1670	5.242	7.113	0.15	44.3
CEERS 1019	8.679	6.954	1.3	45.16
COSW-106725	7.65	6.806	1	44.9
Abell2744-QSO1	7.045	7.477	0.3	45.0
UNCOVER-20466	8.50	8.16	0.356	45.811

Table 7: Predicted radio flux range for recently observed galaxies.

Predicted radio flux range for six fundamental planes					
Source ID	Redshift z	Log (M_{BH}) ($M_\odot$)	L/L $_{Edd}$	Radio flux at 0.1 GHz (nJy)	Radio flux at 10 GHz (nJy)
10013704	5.919	5.65	1.06	10-100	0.3-30
8083	4.6482	7.25	0.16	400-6000	20-300
3608	5.268	6.82	0.11	90-1000	0.3-4
11836	4.409	7.13	0.2	400-5000	20-250
20621	4.681	7.3	0.18	500-8000	20-320
73488	4.1332	7.71	0.16	1800-30000	70-1200
77652	5.229	6.86	0.38	200-2200	9-100
61888	5.874	7.22	0.32	300-5000	15-250
62309	5.172	6.56	0.39	80-1000	7-90
53757	4.4480	7.69	0.05	800-14000	35-700
954	6.760	7.9	0.42	1500-30000	70-1500
GN-z11	10.6	6.2	5.5	30-300	15-150
UHZ1	10.3	7.602	1	400-10000	20-400
CEERS 1670	5.242	7.113	0.15	200-3000	8-130
CEERS 1019	8.679	6.954	1.3	150-2000	6-90
COSW-106725	7.65	6.806	1	100-1500	5-75
Abell2744-QSO1	7.045	7.477	0.3	400-7000	17-300
UNCOVER-20466	8.50	8.16	0.356	1800-40000	70-1500

Table 8: Predictions for the detection by SKA for newly observed galaxies.

			1 hour intgration time				10 hour intgration time				100 hour intgration time			
Source ID/ Frequency (GHZ)	Red shift z	Log (M_{BH}) (M_{Θ})	0.1 - 0.3	0.3 - 1.05	0.95 - 1.76	5.8 - 10	0.1 - 0.3	0.3 - 1.05	0.95 - 1.76	5.8 - 10	0.1 - 0.3	0.3 - 1.05	0.95 - 1.76	5.8 - 10
10013704	5.919	5.65												
8083	4.6482	7.25									✓	✓	✓	✓
3608	5.268	6.82												
11836	4.409	7.13											✓	✓
20621	4.681	7.3										✓	✓	✓
73488	4.133	7.71					✓	✓	✓	✓	✓	✓	✓	✓
77652	5.229	6.86												✓
61888	5.874	7.22										✓	✓	✓
62309	5.17	6.56												
53757	4.44	7.69									✓	✓	✓	✓
954	6.76	7.9					✓	✓	✓	✓	✓	✓	✓	✓
GN-z11	10.6	6.2												
UHZ1	10.3	7.602									✓	✓	✓	✓
CEERS 1670	5.242	7.113											✓	✓
CEERS 1019	8.679	6.954												
COSW- 106725	7.65	6.806												
Abell2744- QSO1	7.045	7.477									✓	✓	✓	✓
UNCOVER- 20466	8.50	8.16			✓	✓	✓	✓	✓	✓	✓	✓	✓	✓

Table 9: Predictions for the detection by ngVLA for newly observed galaxies.

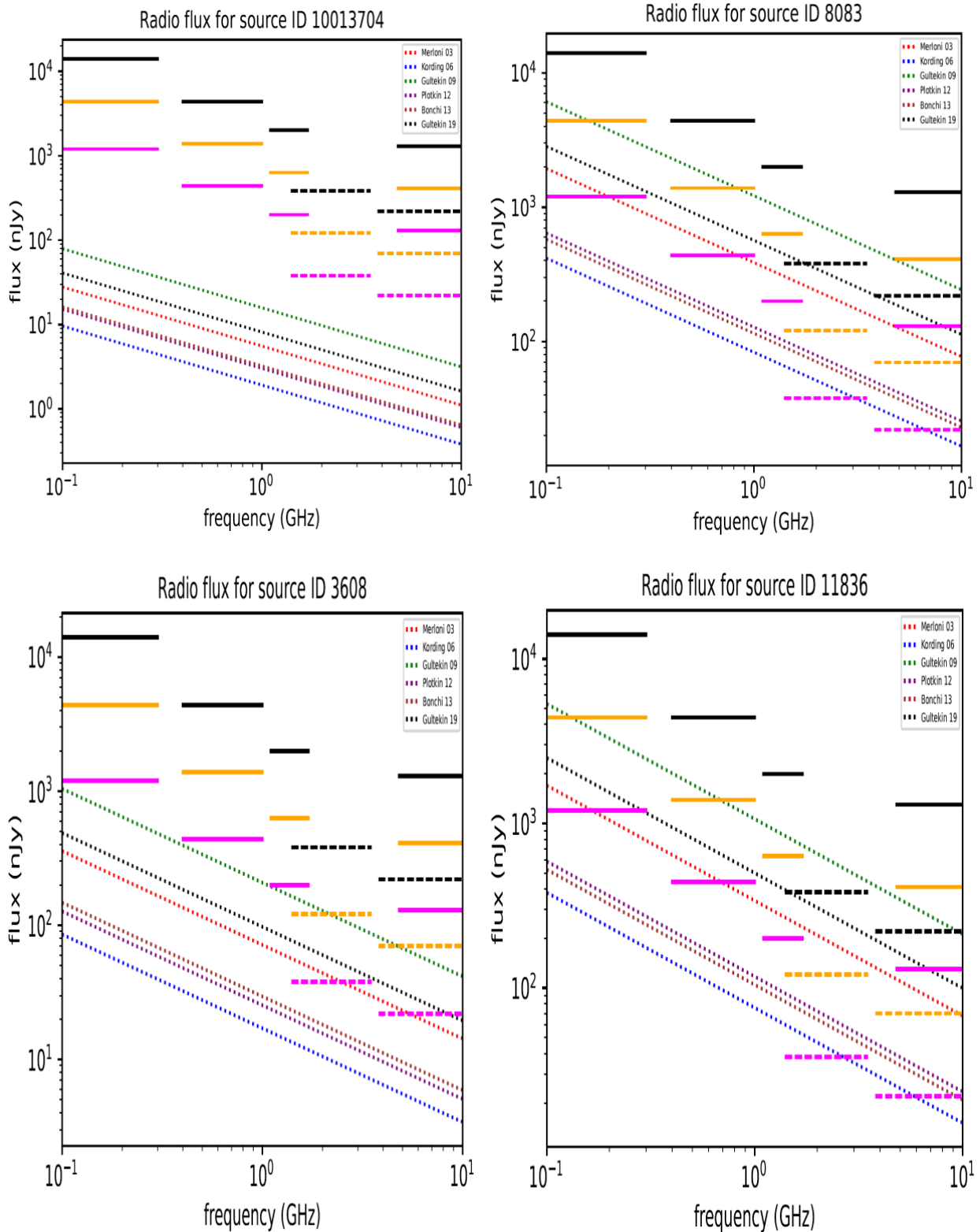| Prections for detection by ngVLA								
			1 hour intgration time		10 hour intgration time		100-hour integration time	
Source ID	Redshift z	Log (M_{BH}) (M_Θ)	1.2-3.5 GHz	3.6-10 GHz	1.2-3.5 GHz	3.6-10 GHz	1.2-3.5 GHz	3.6-10 GHz
10013704	5.919	5.65						
8083	4.6482	7.25			✓	✓	✓	✓
3608	5.268	6.82					✓	✓
11836	4.409	7.13			✓	✓	✓	✓
20621	4.681	7.3			✓	✓	✓	✓
73488	4.1332	7.71	✓	✓	✓	✓	✓	✓
77652	5.229	6.86			✓	✓	✓	✓
61888	5.874	7.22			✓	✓	✓	✓
62309	5.172	6.56					✓	✓
53757	4.4480	7.69	✓	✓	✓	✓	✓	✓
954	6.760	7.9	✓	✓	✓	✓	✓	✓
GN-z11	10.6	6.2						
UHZ1	10.3	7.602			✓	✓	✓	✓
CEERS 1670	5.242	7.113			✓	✓	✓	✓
CEERS 1019	8.679	6.954					✓	✓
COSW-106725	7.65	6.806					✓	✓
Abell2744-QSO1	7.045	7.477			✓	✓	✓	✓
UNCOVER-20466	8.50	8.16	✓	✓	✓	✓	✓	✓

Figure 19: Estimated radio flux for newly observed galaxies. These galaxies are observed by JWST for the data given in Table 6 with telescope limits for SKA and ngVLA. The dashed lines show telescope limits for ngVLA, and the solid line is for SKA. The pink color is for 100-hour integration time, orange is for 10-hour integration time, and black is for 1-hour integration time.
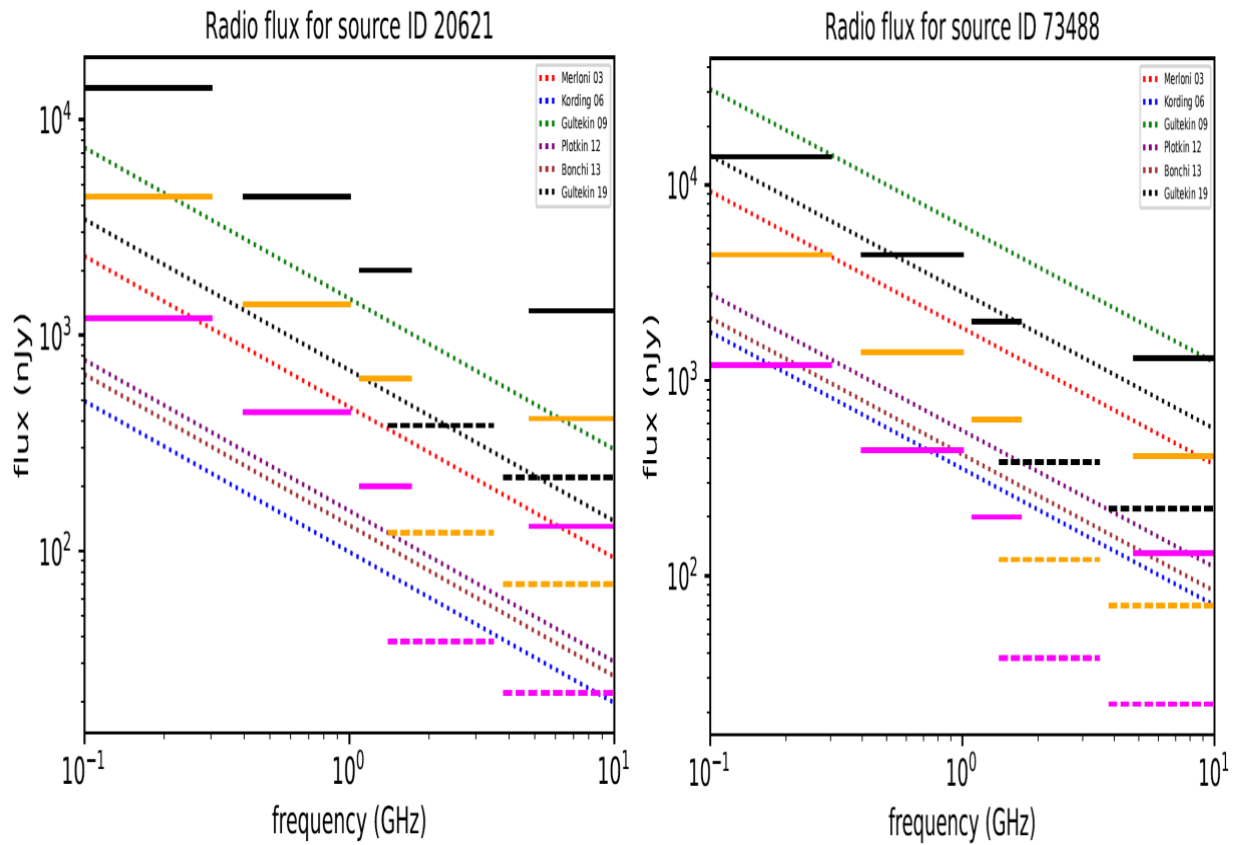
Figure 19: Estimated radio flux for newly observed galaxies (Continued). These galaxies are observed by JWST for the data given in Table 6 with telescope limits for SKA and ngVLA. The dashed lines show telescope limits for ngVLA, and the solid line is for SKA. The pink color is for 100-hour integration time, orange is for 10-hour integration time, and black is for 1-hour integration time.

Figure 19: Estimated radio flux for newly observed galaxies (Continued). These galaxies are observed by JWST for the data given in Table 6 with telescope limits for SKA and ngVLA. The dashed lines show telescope limits for ngVLA, and the solid line is for SKA. The pink color is for 100-hour integration time, orange is for 10-hour integration time, and black is for 1-hour integration time.
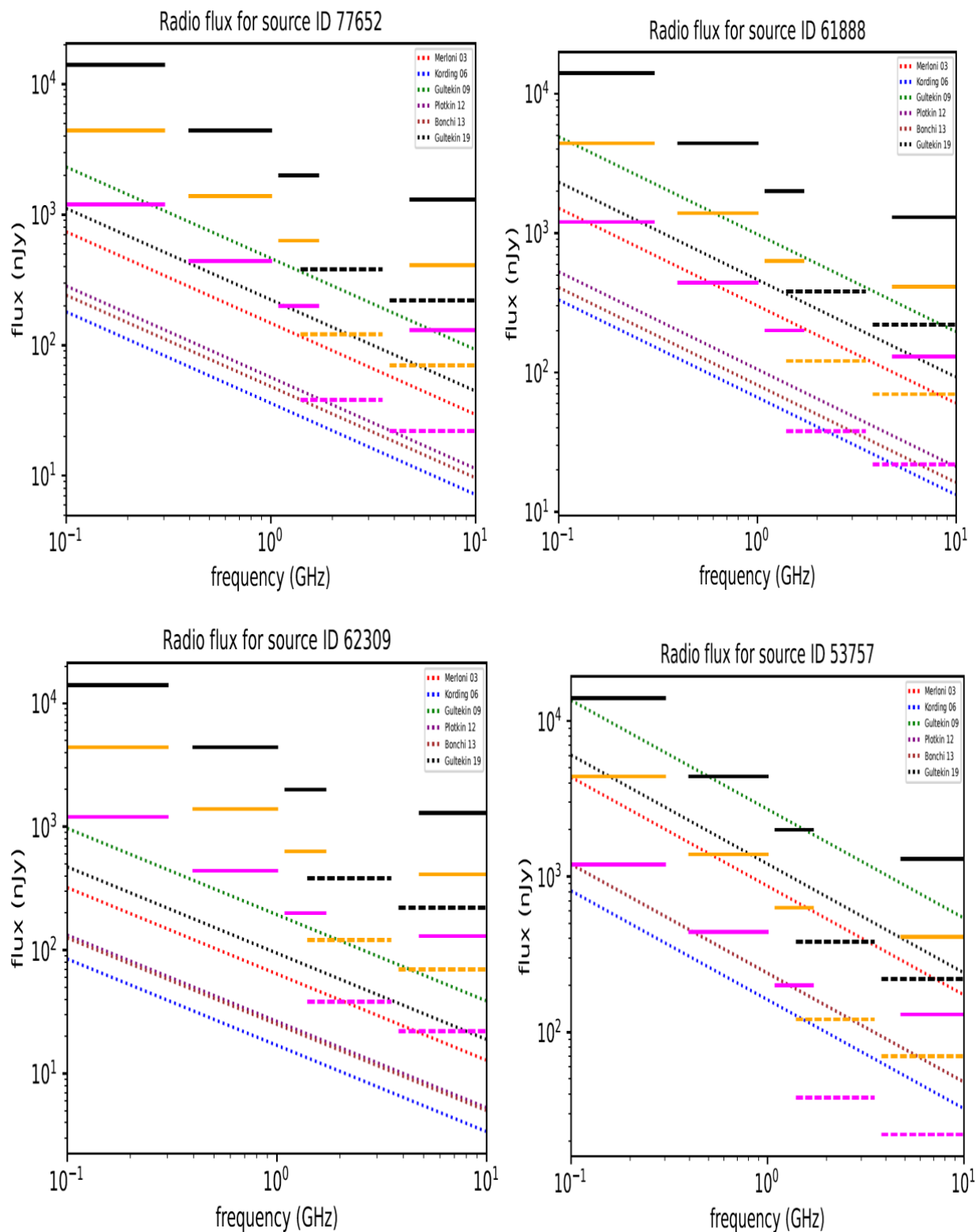
Figure 19: Estimated radio flux for newly observed galaxies (Continued). These galaxies are observed by JWST for the data given in Table 6 with telescope limits for SKA and ngVLA. The dashed lines show telescope limits for ngVLA, and the solid line is for SKA. The pink color is for 100-hour integration time, orange is for 10-hour integration time, and black is for 1-hour integration time.
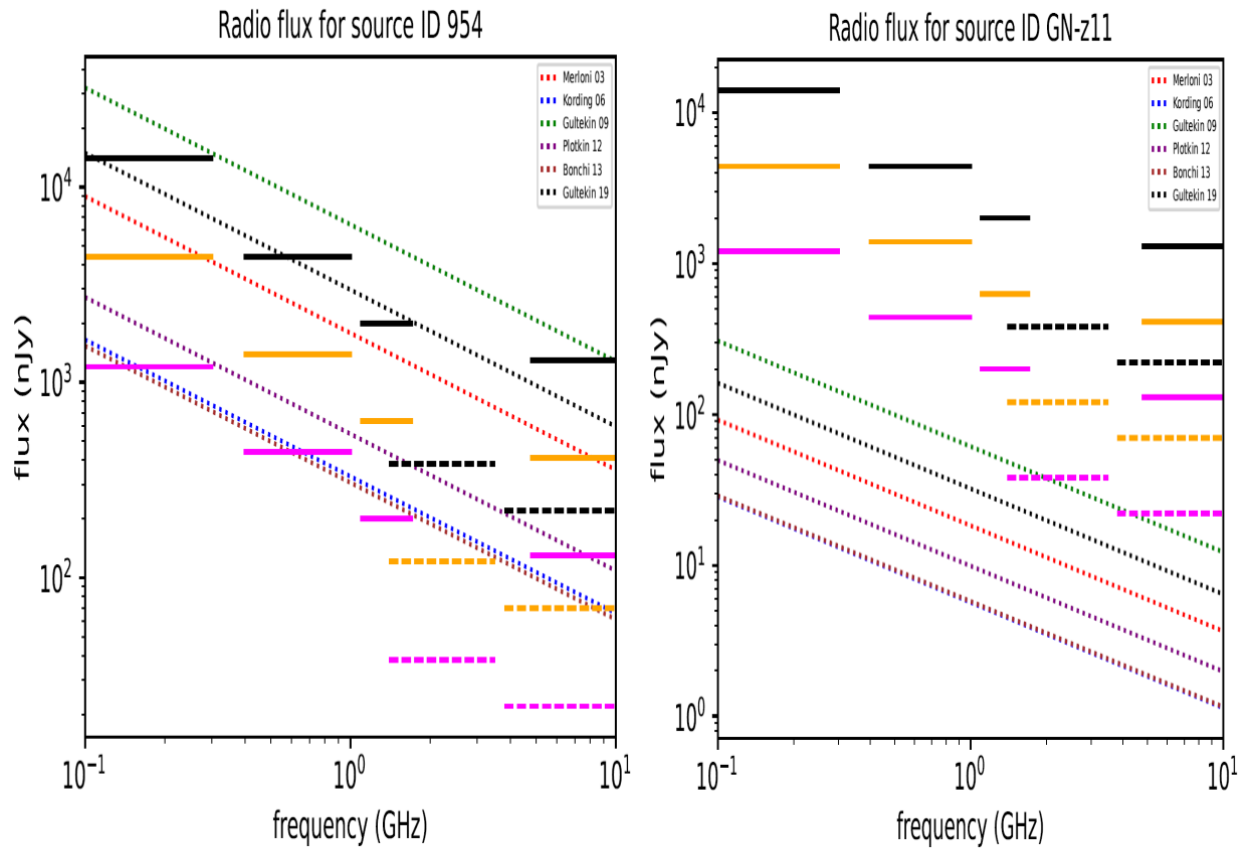
Figure 19: Estimated radio flux for newly observed galaxies (Continued). These galaxies are observed by JWST for the data given in Table 6 with telescope limits for SKA and ngVLA. The dashed lines show telescope limits for ngVLA, and the solid line is for SKA. The pink color is for 100-hour integration time, orange is for 10-hour integration time, and black is for 1-hour integration time.
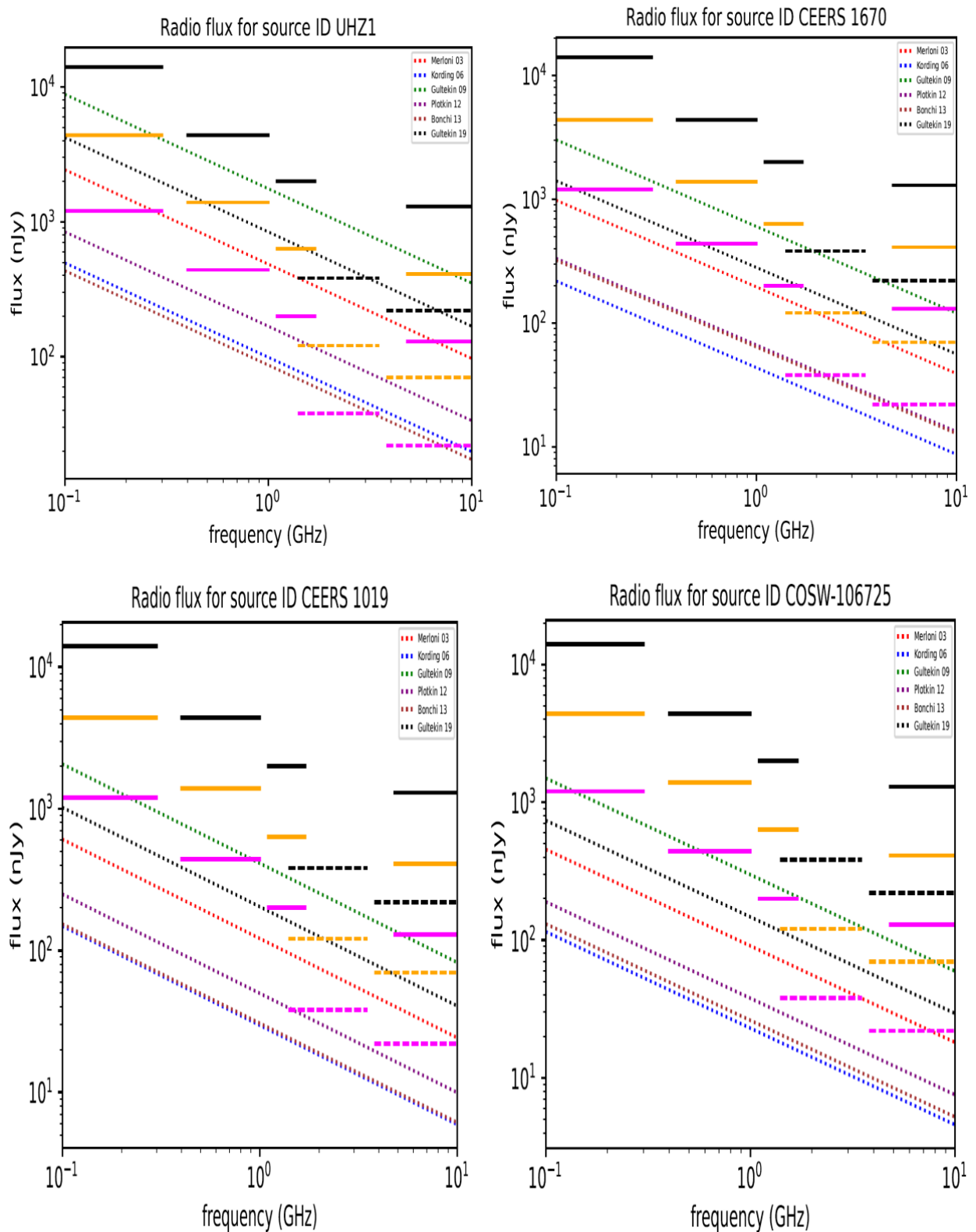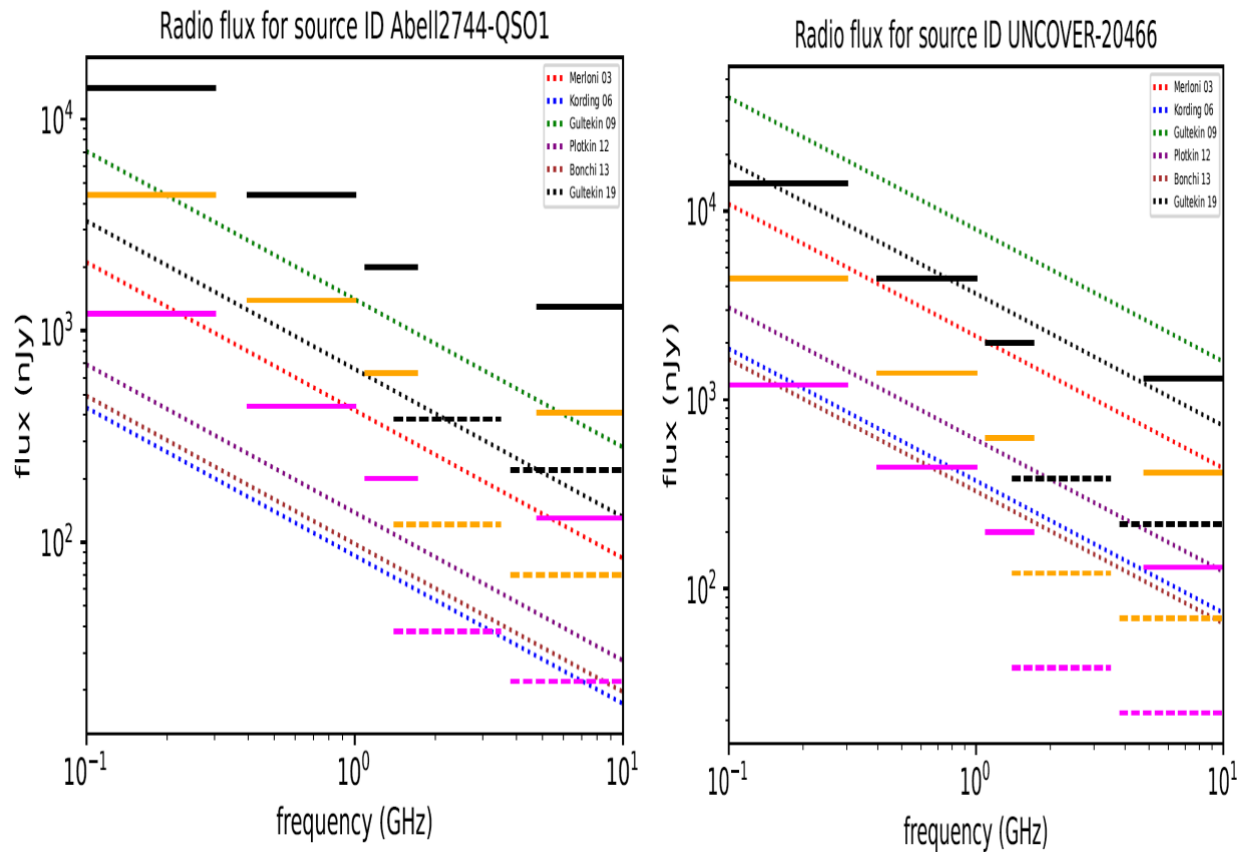
Figure 19: Estimated radio flux for newly observed galaxies (Continued). These galaxies are observed by JWST for the data given in Table 6 with telescope limits for SKA and ngVLA. The dashed lines show telescope limits for ngVLA, and the solid line is for SKA. The pink color is for 100-hour integration time, orange is for 10-hour integration time, and black is for 1-hour integration time.

Chapter 5: Conclusions

5.1 Conclusions

The observational study of AGN with low-mass black holes can provide useful constraints on the initial conditions of galaxy evolution. Studying radio emission from low-mass AGN is vital to understanding the evolution of supermassive DCBH. In our study we estimated radio flux for DCBH with mass 10^7 M$_\odot$ at redshift 10 accreting at Eddington accretion rate. The main motivation for choosing high redshift is that at low redshift star formation rates are high so it's not convenient to distinguish flux from HII regions, and Supernova remnants from the core and jets of the accreting BH. Our estimates for radio flux clearly show that at high redshift the flux from the core and jet of the DCBH can be easily distinguished from the flux from HII regions and Supernova Remnants as the range for the flux from the core for different fundamental planes is between 100 nJy and 2000 nJy while the flux HII regions are only a few nJy and flux from supernova remnants is 40nJy. The flux from the jet of the BH is quite high compared to the core as the jet power for BH of mass 10^7 M$_\odot$ at redshift 10 accreting at Eddington accretion rate is 10^{45} erg/s which is quite high.

According to recent research, AGN may be detectable in the near-infrared by the James Webb Space Telescope, Euclid, and the Roman Space Telescope. Several studies have looked into the possibility of supermassive DCBHs being detected in the near-infrared (NIR) by the James Webb Space Telescope (JWST), Euclid, and the Roman Space Telescope (RST). They discovered that DCBHs might be detected by JWST at z = 20 and by Euclid and RST at z = 6 - 8, with lensing by galaxy clusters and large galaxies in their wide fields extending detections up to z 10 - 15 (Whalen et al., 2020; Barrow et al., 2018). New radio telescopes with unparalleled sensitivity, such as the Square Kilometer Array (SKA) and the Next-Generation Very Large Array (NGVLA), are being built and they will be making observations in a decade. Using our estimates, we made predictions for the upcoming telescopes for different integration times. It is concluded that a BH with mass 10^7 M$_\odot$ at redshift 10 accreting at Eddington accretion rate can be detected with ngVLA when the integration time is set to 100 hours while it cannot be detected with SKA but

increasing the integration time can help us observe it with SKA as well as shown in Figure 18.

We also compared flux for BHs with different masses and made predictions for SKA and ngVLA. Figure 13 clearly shows that SKA and ngVLA cannot detect BHs with masses less than 10^7 $M_\odot$ accreting at Eddington accretion rate at redshift 10 as more massive BHs emit more radio flux compared to less massive BHs. While flux may vary depending on the accretion rate, increasing the accretion rate increases the flux. So BHs with lower masses may be detected by SKA and ngVLA if they are accreting at higher rates as shown in Figure 16 that those fundamental planes that were not detectable by SKA before can be detected if they are accreting at super Eddington accretion rates.

We also estimated flux for BHs with masses ranging from 10^5 to 10^7 $M_\odot$ at a range of redshifts varying from 20-6. The ngVLA with 100 hours integration time could detect DCBHs during birth at z = 8 - 9 when their comoving number densities were highest (Valiante et al., 2017), but it could only detect more massive, evolved BHs at greater redshifts. BHs with masses less than 10^7 $M_\odot$ accreting at Eddington accretion rate cannot be detected with either SKA or ngVLA.

Recent studies suggest that DCBHs could be detected in the near-infrared by the James Webb Space Telescope, Euclid, and the Roman Space Telescope. Several studies have examined the prospects for the detection of supermassive DCBHs in the near-infrared (NIR) by the James Webb Space Telescope (JWST), Euclid, and the Roman Space Telescope (RST) (Whalen et al., 2020; Barrow et al., 2018). We extended our work and predicted the radio flux for newly observed galaxies by JWST. We took data from (Maiolino et al., 2023) and (Scoggins & Haiman, 2023) for these newly observed galaxies and predicted Radio flux from the accretion disk of the black holes. Radio flux from these BHs may be contaminated by emission from H II regions and SNRs in their host galaxies, which would host active star formation, but we cannot estimate the radio flux from HII regions and Supernova remnants as star formation rates for these galaxies are still not available as they have been recently observed and are still being studied. Our model predicts that sources with source ID 73488,954, UNCOVER-20466 (Maiolino et al., 2023;

Scoggins & Haiman, 2023) can be easily detected with SKA and ngVLA with 100 hours of integration time.

5.2 Future work

Moving forward, there are numerous opportunities for research and exploration of low-mass AGN. Although we tried to develop a comprehensive theoretical model that can make predictions for upcoming advanced radio telescopes, some areas can still be further extended to give a better understanding of low-mass AGN. In our model, we considered fixed BH masses while this is not the actual scenario. The mass of an accreting BH constantly changes depending on the accretion rate. We can extend the scope of our work by taking the change in mass into consideration by looking at its accretion rate.

We estimated the radio flux for the newly observed galaxies by JWST and made predictions for the detection by SKA and ngVLA but since these are newly observed galaxies and much information is not available presently so we can improve our predictions in the future as more work will be done and more information will be available. Specifically, we couldn't estimate the radio flux from HII regions and Supernova remnants as star formation rates for these galaxies are not available. In the future when star formation rates are available we can estimate the flux using our model and predict if the flux from AGN is contaminated by emission from H II regions and SNRs in their host galaxies or not which will in turn improve our understanding of the formation and evolution mechanisms.

References

Barrow, K. S. S., Aykutalp, A., & Wise, J. H. (2018). Observational signatures of massive black hole formation in the early universe. *Nature Astronomy*, *2*(12), 987–994. https://doi.org/10.1038/s41550-018-0569-y

Bear, E., & Soker, N. (2020). Jet-driven active galactic nucleus feedback in galaxy formation before black hole formation. *New Astronomy*, *81*, 101438. https://doi.org/10.1016/j.newast.2020.101438

Bonchi, A., La Franca, F., Melini, G., Bongiorno, A., & Fiore, F. (2013). On the radio luminosity distribution of active galactic nuclei and the black hole fundamental plane. *Monthly Notices of the Royal Astronomical Society*, *429*(3), 1970–1980. https://doi.org/10.1093/mnras/sts456

Casares, J., & Jonker, P. G. (2014). Mass Measurements of Stellar and Intermediate Mass Black-Holes. *Space Science Reviews*, *183*(1–4), 223–252. https://doi.org/10.1007/s11214-013-0030-6

Cattaneo, A., Dekel, A., Devriendt, J., Guiderdoni, B., & Blaizot, J. (2006). Modelling the galaxy bimodality: Shutdown above a critical halo mass: Modelling the galaxy bimodality. *Monthly Notices of the Royal Astronomical Society*, *370*(4), 1651–1665. https://doi.org/10.1111/j.1365-2966.2006.10608.x

Cresci, G., & Maiolino, R. (2018). Observing positive and negative AGN feedback. *Nature Astronomy*, *2*(3), 179–180. https://doi.org/10.1038/s41550-018-0404-5

Croton, D. J., Springel, V., White, S. D. M., De Lucia, G., Frenk, C. S., Gao, L., Jenkins, A., Kauffmann, G., Navarro, J. F., & Yoshida, N. (2006). The many lives of active galactic nuclei: Cooling flows, black holes and the luminosities and colours of galaxies. *Monthly Notices of the Royal Astronomical Society*, *365*(1), 11–28. https://doi.org/10.1111/j.1365-2966.2005.09675.x

De Gasperin, F., Intema, H. T., & Frail, D. A. (2018). A radio spectral index map and catalogue at 147–1400 MHz covering 80 per cent of the sky. *Monthly Notices of the Royal Astronomical Society*, *474*(4), 5008–5022. https://doi.org/10.1093/mnras/stx3125

Dong, X.-B., Ho, L. C., Yuan, W., Wang, T.-G., Fan, X., Zhou, H., & Jiang, N. (2012). A uniformly selected sample of low-mass black holes in seyfert 1 galaxies. *The Astrophysical Journal*, *755*(2), 167. https://doi.org/10.1088/0004-637X/755/2/167

Fabian, A. C., & Lasenby, A. N. (2019). *Astrophysical Black Holes* (arXiv:1911.04305). arXiv. http://arxiv.org/abs/1911.04305

Greene, J. E. (2012). Low-mass black holes as the remnants of primordial black hole formation. *Nature Communications*, *3*(1), 1304. https://doi.org/10.1038/ncomms2314

Greene, J. E., & Ho, L. C. (2004). Active Galactic Nuclei with Candidate Intermediate-Mass Black Holes. *The Astrophysical Journal*, *610*(2), 722–736. https://doi.org/10.1086/421719

Greene, J. E., & Ho, L. C. (2007). A New Sample of Low-Mass Black Holes in Active Galaxies. *The Astrophysical Journal*, *670*(1), 92–104. https://doi.org/10.1086/522082

Greene, J. E., Strader, J., & Ho, L. C. (2020). Intermediate-Mass Black Holes. *Annual Review of Astronomy and Astrophysics*, *58*(1), 257–312. https://doi.org/10.1146/annurev-astro-032620-021835

Gültekin, K., Cackett, E. M., King, A. L., Miller, J. M., & Pinkney, J. (2014). Low-mass agns and their relation to the fundamental plane of black hole accretion. *The Astrophysical Journal*, *788*(2), L22. https://doi.org/10.1088/2041-8205/788/2/L22

Gültekin, K., Cackett, E. M., Miller, J. M., Di Matteo, T., Markoff, S., & Richstone, D. O. (2009). The fundamental plane of accretion onto black holes with dynamical masses. *The Astrophysical Journal*, *706*(1), 404–416. https://doi.org/10.1088/0004-637X/706/1/404

Gültekin, K., King, A. L., Cackett, E. M., Nyland, K., Miller, J. M., Matteo, T. D., Markoff, S., & Rupen, M. P. (2019). The Fundamental Plane of Black Hole Accretion and Its Use as a Black Hole-Mass Estimator. *The Astrophysical Journal*, *871*(1), 80. https://doi.org/10.3847/1538-4357/aaf6b9

Harada, T., Yoo, C.-M., Kohri, K., & Nakao, K.-I. (2017). Spins of primordial black holes formed in the matter-dominated phase of the Universe. *Physical Review D*, *96*(8), 083517. https://doi.org/10.1103/PhysRevD.96.083517

Johnson, J. L., Khochfar, S., Greif, T. H., & Durier, F. (2011). Accretion on to black holes formed by direct collapse: Accretion on to black holes. *Monthly Notices of the Royal Astronomical Society*, *410*(2), 919–933. https://doi.org/10.1111/j.1365-2966.2010.17491.x

Körding, E., Falcke, H., & Corbel, S. (2006). Refining the fundamental plane of accreting black holes. *Astronomy & Astrophysics*, *456*(2), 439–450. https://doi.org/10.1051/0004-6361:20054144

Kormendy, J., & Ho, L. C. (2013). Coevolution (Or Not) of Supermassive Black Holes and Host Galaxies. *Annual Review of Astronomy and Astrophysics*, *51*(1), 511–653. https://doi.org/10.1146/annurev-astro-082708-101811

Latif, M. A., & Ferrara, A. (2016). Formation of Supermassive Black Hole Seeds. *Publications of the Astronomical Society of Australia*, *33*, e051. https://doi.org/10.1017/pasa.2016.41

Latif, M. A., & Khochfar, S. (2020). Inception of a first quasar at cosmic dawn. *Monthly Notices of the Royal Astronomical Society*, *497*(3), 3761–3769. https://doi.org/10.1093/mnras/staa2218

Latif, M. A., Schleicher, D. R. G., & Schmidt, W. (2014). Magnetic fields during the formation of supermassive black holes. *Monthly Notices of the Royal Astronomical Society*, *440*(2), 1551–1561. https://doi.org/10.1093/mnras/stu357

Maiolino, R., Scholtz, J., Curtis-Lake, E., Carniani, S., Baker, W., de Graaff, A., Tacchella, S., Übler, H., D'Eugenio, F., Witstok, J., Curti, M., Arribas, S., Bunker, A. J., Charlot, S., Chevallard, J., Eisenstein, D. J., Egami, E., Ji, Z., Jones, G. C., … Willott, C. (2023). *JADES. The diverse population of infant Black Holes at 4<z<11: Merging, tiny, poor, but mighty* (arXiv:2308.01230). arXiv. http://arxiv.org/abs/2308.01230

Marconi, A., Risaliti, G., Gilli, R., Hunt, L. K., Maiolino, R., & Salvati, M. (2004). Local supermassive black holes, relics of active galactic nuclei and the X-ray background. *Monthly Notices of the Royal Astronomical Society*, *351*(1), 169–185. https://doi.org/10.1111/j.1365-2966.2004.07765.x

Martinelli, M., Scarcella, F., Hogg, N. B., Kavanagh, B. J., Gaggero, D., & Fleury, P. (2022). Dancing in the dark: Detecting a population of distant primordial black holes. *Journal of Cosmology and Astroparticle Physics*, *2022*(08), 006. https://doi.org/10.1088/1475-7516/2022/08/006

Merloni, A., Heinz, S., & Di Matteo, T. (2003). A Fundamental Plane of black hole activity. *Monthly Notices of the Royal Astronomical Society*, *345*(4), 1057–1076. https://doi.org/10.1046/j.1365-2966.2003.07017.x

Mezcua, M. (2017). Observational evidence for intermediate-mass black holes. *International Journal of Modern Physics D*, *26*(11), 1730021. https://doi.org/10.1142/S021827181730021X

Mezcua, M., & Domínguez Sánchez, H. (2020). Hidden AGNs in Dwarf Galaxies Revealed by MaNGA: Light Echoes, Off-nuclear Wanderers, and a New Broad-line AGN. *The Astrophysical Journal*, *898*(2), L30. https://doi.org/10.3847/2041-8213/aba199

Mezcua, M., & Prieto, M. A. (2014). Evidence of parsec-scale jets in low-luminosity active galactic nuclei. *The Astrophysical Journal*, *787*(1), 62. https://doi.org/10.1088/0004-637X/787/1/62

Miller, J. M. (2007). Relativistic X-Ray Lines from the Inner Accretion Disks Around Black Holes. *Annual Review of Astronomy and Astrophysics*, *45*(1), 441–479. https://doi.org/10.1146/annurev.astro.45.051806.110555

Panessa, F., Baldi, R. D., Laor, A., Padovani, P., Behar, E., & McHardy, I. (2019). *The Origin of Radio Emission from Radio-Quiet AGN* (arXiv:1902.05917). arXiv. http://arxiv.org/abs/1902.05917

Plotkin, R. M., Markoff, S., Kelly, B. C., Körding, E., & Anderson, S. F. (2012). Using the Fundamental Plane of black hole activity to distinguish X-ray processes from weakly accreting black holes: Distinguishing black hole X-ray processes. *Monthly Notices of the Royal Astronomical Society*, *419*(1), 267–286. https://doi.org/10.1111/j.1365-2966.2011.19689.x

Plotkin, R. M., & Reines, A. E. (2018). *Science with an ngVLA: Local Constraints on Supermassive Black Hole Seeds* (arXiv:1810.06814). arXiv. http://arxiv.org/abs/1810.06814

Scoggins, M. T., & Haiman, Z. (2023). *Diagnosing the massive-seed pathway to high-redshift black holes: Statistics of the evolving black hole to host galaxy mass ratio* (arXiv:2310.00202). arXiv. http://arxiv.org/abs/2310.00202

Smolčić, V., Zamorani, G., Schinnerer, E., Bardelli, S., Bondi, M., Bîrzan, L., Carilli, C. L., Ciliegi, P., Elvis, M., Impey, C. D., Koekemoer, A. M., Merloni, A., Paglione, T., Salvato, M., Scodeggio, M., Scoville, N., & Trump, J. R. (2009). Cosmic evolution of radio selected active galactic nuclei in the cosmos field. *The Astrophysical Journal*, *696*(1), 24–39. https://doi.org/10.1088/0004-637X/696/1/24

Tremaine, S. (2014). The Odd Couple: Quasars & Black Holes. *Daedalus*, *143*(4), 103–113. https://doi.org/10.1162/DAED_a_00310

Valiante, R., Agarwal, B., Habouzit, M., & Pezzulli, E. (2017). On the formation of the first quasars. *Publications of the Astronomical Society of Australia*, *34*, e031. https://doi.org/10.1017/pasa.2017.25

Vito, F., Di Mascia, F., Gallerani, S., Zana, T., Ferrara, A., Carniani, S., & Gilli, R. (2022). Feedback effect on the observable properties of $z>6$ AGN. *Monthly Notices of the Royal Astronomical Society*, *514*(2), 1672–1688. https://doi.org/10.1093/mnras/stac1422

Whalen, D. J., Latif, M. A., & Mezcua, M. (2023). *Radio Emission From a $z =$ 10.1 Black Hole in UHZ1* (arXiv:2308.03837). arXiv. http://arxiv.org/abs/2308.03837

Whalen, D. J., Mezcua, M., Meiksin, A., Hartwig, T., & Latif, M. A. (2020). Radio Power from a Direct-collapse Black Hole in CR7. *The Astrophysical Journal Letters*, *896*(2), L45. https://doi.org/10.3847/2041-8213/ab9a30

Whalen, D. J., Mezcua, M., Patrick, S. J., Meiksin, A., & Latif, M. A. (2021). Radio
    Power from Direct-Collapse Black Holes. *The Astrophysical Journal Letters*,
    922(2), L39. https://doi.org/10.3847/2041-8213/ac35e6

Yue, B., & Ferrara, A. (2021). Radio signals from early direct collapse black holes.
    Monthly Notices of the Royal Astronomical Society, *506*(4), 5606–5618.
    https://doi.org/10.1093/mnras/stab2121

Zahid, M., Rayimbaev, J., Sarikulov, F., Khan, S. U., & Ren, J. (2023). Shadow of
    rotating and twisting charged black holes with cloud of strings and quintessence.
    The European Physical Journal C, *83*(9), 855.
    https://doi.org/10.1140/epjc/s10052-023-12025-5

UAE UNIVERSITY MASTER THESIS NO. 2023: 142

In this thesis we estimated the Radio emission from low-mass Active Galactic nuclei by developing a theoretical model. This model was then applied to recently observed galaxies by James Web Space Telescope and predictions were made for their detection by upcoming telescopes such as Square Kilometer Arraya and New Generation Very Large Array.

Ammara Aftab received her Master of Science in Space Sciences from the Department of Physics, College of Science, United Arab Emirates University and her Bachelor of Science in Physics from International Islamic University Islamabad, Pakistan.

www.uaeu.ac.ae